Hindawi
Discrete Dynamics in Nature and Society
Volume 2022, Article ID 8504993, 27 pages
https://doi.org/10.1155/2022/8504993

Research Article

Stability Analysis and Optimal Control of a Limnothrissa Miodon Model with Harvesting

Farikayi K. Mutasa,[1] **Brian Jones**,[2] **Senelani D. Hove-Musekwa**,[1] **Itai H. Tendaupenyu**,[3] **Tamuka Nhiwatiwa**,[4] **and Mzime R. Ndebele-Murisa**[5]

[1]*Department of Applied Mathematics, National University of Science and Technology, P.O. Box AC939 Ascot, Bulawayo, Zimbabwe*
[2]*Department of Statistics and Operations Research, National University of Science and Technology, P.O. Box AC939 Ascot, Bulawayo, Zimbabwe*
[3]*The Zimbabwe Parks and Wildlife Management Authority, Cnr Sandringham & Borrowdale Rd, Botanical Gardens, P.O. Box CY140, Causeway, Harare, Zimbabwe*
[4]*Department of Biological Sciences, University of Zimbabwe, P.O. MP167 Mt. Pleasant, Harare, Zimbabwe*
[5]*School of Wildlife and Ecology, Chinhoyi University of Technology, Chinhoyi, Zimbabwe*

Correspondence should be addressed to Farikayi K. Mutasa; farikayi.mutasa@nust.ac.zw

Received 19 November 2021; Accepted 18 March 2022; Published 5 May 2022

Academic Editor: Leonid Shaikhet

We construct a theoretical, deterministic mathematical model of the dynamics of Limnothrissa miodon with nutrients, phytoplankton, and zooplankton and investigate the effect of harvesting on the population density of Limnothrissa miodon in a lake. For the autonomous model, results from local stability analysis are in agreement with numerical simulations in that the coexistence equilibrium is locally stable, provided certain conditions are satisfied. The coexistence equilibrium is globally unstable if it is feasible. Numerical results show that a stable limit cycle exists for the nonautonomous model. Optimal control results show an optimal harvesting monthly effort of 15394 boat nights which corresponds to 505 fishing units, showing that there is overcapacity in Lake Kariba. A maximum sustainable annual catch of 34669 tonnes is obtained and simulation results show that Limnothrissa miodon abundance is more closely related to nutrient inflow than to harvesting.

1. Introduction

Limnothrissa miodon (Boulenger, 1906), also referred to as kapenta, is a major source of protein and income to fishing cooperatives, wholesalers, retailers, and the local community [1]. Management of the Lake Kariba fishery which is shared by both Zimbabwe and Zambia is of paramount importance for the continued survival of the kapenta [2, 3]. Harvesting of kapenta by fishing vessels plays an important role in the dynamics of the sardine Limnothrissa miodon [2, 3] and as a result, it is critical to look into the role of harvesting in its dynamics theoretically and numerically. Harvesting of the natural resource needs to be done in a sustainable manner so that it is not overexploited and becomes extinct. Therefore, mathematical modelling of the Limnothrissa miodon model with harvesting will provide insight into the kapenta fishery dynamics in Lake Kariba. A deterministic model involving nutrients, plankton, and Limnothrissa miodon, as well as harvesting by fishing vessels, has yet to be developed and analysed. We present and analyze a deterministic continuous dynamical system composed of ordinary differential equations that describe the dynamics of Limnothrissa miodon in the presence of nutrients, plankton, and harvesting. The Limnothrissa miodon model will aid us in our understanding of the dynamics of the aquatic ecosystem in the kapenta fishery in Lake Kariba.

According to McLachlan [4], the lake productivity is largely due to reloading of nutrients at turnover, the

nutrient-rich sediment carried by the inflowing rivers, and the nutrients discharged as runoff into the lake. The lake loses large amounts of nutrients per year since it experiences large outflows of between 50 and 60 km^3 as compared to its volume of 160 km^3 [5]. Marshall [6] estimated the total mortality of Limnothrissa miodon to be 0.816 $month^{-1}$ and 1.149 $month^{-1}$ in 1978 and 1983, respectively. Moreau et al. [7] estimated the total mortality of Limnothrissa miodon to be between 0.37 $month^{-1}$ and 0.81 $month^{-1}$ in Lake Tanganyika. For Lake Kariba and Lake Tanganyika, the natural mortality rates for Limnothrissa miodon were 0.44 and 0.30 $month^{-1}$, respectively, and Pauly's empirical method was used to estimate the parameters. According to Marshall [6], the fishing effort to mortality relationship of Limnothrissa miodon is 0.731 $month^{-1}$. From the biomass assessment done in 1994/95, the fishing mortality was estimated to be 2.06 $year^{-1}$ and 2.18 $year^{-1}$ for 1993 and 1994, respectively, for kapenta [8]. The Working Group Assessment [9] obtained a fishing mortality of 2.1 $year^{-1}$, a natural mortality of 3.5 $year^{-1}$, giving a total mortality of 5.6 $year^{-1}$ for kapenta in Lake Kariba. Cochrane [10] and Marshall [11] concluded that catches of Limnothrissa miodon vary seasonally with availability of food. The fish are more abundant after turnover in August to September and after the annual flooding of the inflowing rivers in April and May. Marshall [11] also concluded the existence of a possible relationship between the sardine biomass and fishing effort. In their study on the impact of fishing pressure on kapenta production on the Zambian side of Lake Kariba, Chali et al. [2] concluded that both catch per unit effort (CPUE) and kapenta production were declining significantly. Kapenta production and CPUE decreased from 9993 tonnes (t) and 0.145 t/boat/night to 6004 t and 0.085 t/boat/night from 2009 to 2012, respectively. The fishing effort increased from about 68734 to 70706 boat nights from 2009 to 2012, respectively. CPUE is an indirect measure of kapenta abundance in the lake and so a decreasing CPUE shows overexploitation of the sardine. On the Zambian side of the lake, the fishing units increased from 423 in 2009 to 800 in 2013 and this could have led to the decline in the kapenta stocks and overexploitation of the sardine. The low kapenta catches were as a result of a huge rise in the fishing effort which was more than the 500 recommended rigs for the whole lake [12].

Machena et al. [13] from their study on the preliminary assessment of the trophic structure of Lake Kariba concluded that the fishing mortality of Limnothrissa miodon could be increased since it is fairly harvested. Magadza [14] in his study estimated a maximum sustainable yield (MSY) of kapenta to be 40000 t and concluded that the catches of kapenta in the fishery increased logistically from 1974 to about 1990, where the highest catch of 37000 t was recorded and then decreased thereafter. Madamombe [15] for the period 1974 to 1999 used the Pella and Tomlinson production model and obtained a maximum sustainable yield of 23336 t with a corresponding effort of 725 rigs. Mudenda [16] estimated MSY with the Schaeffer and Fox models and obtained 23525 t and 24271 t with a corresponding fishing effort of 108109 and 141243 boat nights, respectively. Mudenda [16] concluded that there was overfishing in the fishery ranging from 21% – 39%. Tendaupenyu and Pyo [17] for the study period 1988 – 2009 used a maximum entropy model and estimated a MSY of 25372 t with a corresponding fishing effort of 109731 boat nights and they concluded that there was overcapacity in Lake Kariba and that the kapenta stock was in decline. The analytical model used by Tendaupenyu and Pyo [17] estimated a fishing mortality of 1.21 $year^{-1}$ compared to the current 0.927 $year^{-1}$. Tendaupenyu and Pyo [17] used a maximum entropy model and estimated an intrinsic growth rate of 0.42 and a carrying capacity of 240500 t for kapenta in Lake Kariba. Tendaupenyu and Pyo [17] estimated a catchability coefficient of 0.00000153 for kapenta from the Walters and Hilborn model. Dynamical systems have not been used to investigate how kapenta fish populations in Lake Kariba are described and influenced by harvesting. We will be able to quantitatively explain the impact of kapenta fish harvesting by developing and analyzing a mathematical model.

The important question is what levels of the fishing effort will lead to a sustained population density of Limnothrissa miodon in the lake and what fishing pressure will result in the extinction of the natural resource. Many fish harvesting models have been formulated and analysed [18–20] and they mainly differ in the harvesting function.

The remainder of this paper describes the study area, data collection, model formulation, positivity and existence of solutions, equilibrium states and their stability, and optimal control in Section 2. The results which include numerical simulations and analysis are presented in Section 3, a detailed discussion is in Section 4, and conclusions are in Section 5.

2. Materials and Methods

2.1. Study Area. Lake Kariba is located on the Zambezi River, in a tropical area with seasonal rainfall between latitudes 1628′ to 1804′ S and longitudes 2642′ to 2903′ *E* [15]. The offshore single-species pelagic kapenta fishery is highly mechanized, using light attraction and lift nets from boats, and is licensed [21]. According to the 2011 Frame survey [22], the fishing units on the Zimbabwean and Zambian sides of Lake Kariba have similar technical efficiencies and harvesting systems. Large circular dip nets and mercury light bulbs are used in the fishing gear to attract the kapenta. The lights used below and above the lake's surface are powered by generators, the number of which varies from rig to rig. To lower or raise the dip net, hydraulic, mechanical, or manual winches are used [8].

2.2. Data Collection. The Lake Kariba Fisheries Research Institute collects data on catch, effort in the experimental gillnet, and inshore artisanal and offshore kapenta fisheries. The catch data is measured in metric tonnes (wet weight) and fishing effort is the number of nights fished. The CPUE is the kapenta catch that is landed by a boat after a night of fishing and is measured in tonnes/boat/night. It is an important parameter in fisheries management as it is an indicator of fish abundance and economic performance of the

fishery [8]. The University of Zimbabwe Lake Kariba Research Institute collects data on the lake's water quality. The data on acoustic surveys of the biomass of kapenta are not often collected because of the lack of equipment and the cost involved and as such a few fishery surveys have been done on Lake Kariba using research vessels. Therefore, data on the biomass of the aquatic ecosystem of Lake Kariba are only limited to the hydroacoustic surveys of 1981, 1982, and 1983 [23]; September 1988 [24]; 1992 [25]; and for the period from 14 to 24 August 2014 [26]. Some data on phytoplankton, zooplankton, and kapenta in Lake Kariba were obtained from Ndebele-Murisa [21]. Some data is missing due to the fact that some of the fish caught in the offshore fishery are sold to buyers by the fishers before they come back to land and therefore are not recorded. As much as 30% of kapenta catch is thought to be sold illegally by boat crews before landing without the knowledge of the owners of the fishing vessels [27].

Figure 1(a) shows the time series plot of total nitrogen and chlorophyll a in μgl^{-1} in Lake Kariba from November 2016 to December 2017. The monthly averages of total nitrogen and chlorophyll a in Lake Kariba from April 2014 to December 2017 are illustrated in Figure 1(b). Figures 1(c) and 1(d) show the time series plot from November 2016 to December 2017 and the monthly averages from April 2014 to December 2017 of zooplankton in Lake Kariba in individuals per litre (ind./l), respectively.

Figure 2(a) shows the number of fishing vessels on the Zimbabwean side of Lake Kariba from 2008 to 2018. The time series plot shows a gradual increase in the number of units from 307 in 2008 to 530 in 2018. Figure 2(b) shows the number of fishing units on the Zambian and Zimbabwean sides of the lake from 1994 to 1999.

Figure 3(a) illustrates the time series plot of Limnothrissa miodon catches and the CPUE from November 2016 to December 2017. The catch and CPUE monthly averages for the period 1974 to 2018 are shown in Figure 3(b). Figures 3(a) and 3(b) are for the Zimbabwean side of the lake. Figure 3(b) shows a small peak in the catches of kapenta around March and a big peak around August. The peak in March is attributed to the inflow of nutrients through the inflowing rivers and the flooding of the Zambezi river and the one in August is due to the reloading of nutrients after the mixing of the lake around July.

The catches of kapenta versus effort are shown in Figure 3(c). Figure 3(d) shows the effort, catch, and the CPUE of kapenta from 1974 to 2011. Figures 3(c) and 3(d) show data from both the Zambian and Zimbabwean sides of Lake Kariba. For the period 1974 to 2011, the global maximum is at an effort of 104131 boat nights giving a catch of 30943 t in 1990.

2.3. Model Equations. The model has four classes: N denotes nutrient concentration, P denotes phytoplankton population density, Z denotes zooplankton population density, and L denotes Limnothrissa miodon population density. Densities in each class are time-dependent and are denoted by $N(t)$, $P(t)$, $Z(t)$, and $L(t)$, respectively. The Limnothrissa miodon model [28] is extended to include harvesting by the fishing vessels. Nutrients are assumed to enter the water body sinusoidally at the rate

$$a\left(1 + b\,\sin\left(\omega t + \varphi_1\right) + c\,\sin\left(2\omega t + \varphi_2\right)\right), \tag{1}$$

where $a, b, c > 0$ are constants, φ_1 and φ_2 are phase angles, and ω is the angular frequency, a constant. φ_2 captures the delay in the lake mixing, ω is the frequency of the periodic input of nutrients, and ab and ac are the overall amplitude of the first and second nutrient periodic inputs, respectively. The first term of (1) represents the inflow of nutrients from river inflow and runoff and the second term of (1) captures the nutrient reloading into the lake which occurs around mid-year. The sinusoidal function in (1) is chosen for its simplicity and its parameters are to be determined by fitting. Natural depletion of nutrients occurs at a constant rate μ_0. Phytoplankton depletes nutrients at a rate of $\sigma_1 NP$. The rate of growth of phytoplankton is $\phi_1\sigma_1 NP$. It is assumed that the depletion rate of phytoplankton caused by mortality is proportional to P. The change in density of the phytoplankton per unit time per zooplankton as the phytoplankton population density changes is of the modified Holling's type-I response [29] and is denoted by $\sigma_2 PZ$ [29]. The conversion coefficient from phytoplankton to zooplankton is ϕ_2. It is assumed that the rate of zooplankton depletion caused by mortality is proportional to Z. The functional response of zooplankton to the Limnothrissa miodon given by $\sigma_3 ZL$ is of the modified Holling's type-I response, which refers to the change in zooplankton density per unit time per Limnothrissa miodon as the zooplankton population density changes. The conversion coefficient from zooplankton to Limnothrissa miodon is phi ϕ_3. It is assumed that the rate of Limnothrissa miodon depletion caused by mortality is proportional to L, and the rate of depletion caused by crowding is proportional to L^2. Kapenta is harvested at a rate $G(t)$. The model structure improves on the Limnothrissa miodon model in [28] and is shown in Figure 4.

We assume the following:

(1) Catch per unit effort of kapenta is proportional to the fish abundance, $(G(t)/E) \propto L(t)$, and can be written as $G(t) = qEL(t)$ [18, 19], where $q \geq 0$ is a fixed constant of proportionality called the catchability coefficient and $E = E(t) \geq 0$ is the fishing effort per unit time.

(2) Pelagic kapenta have schooling behaviour [18].

(3) Fishing using the rigs involves randomly searching for fish.

(4) Every kapenta in the body of water has an equal chance of being captured.

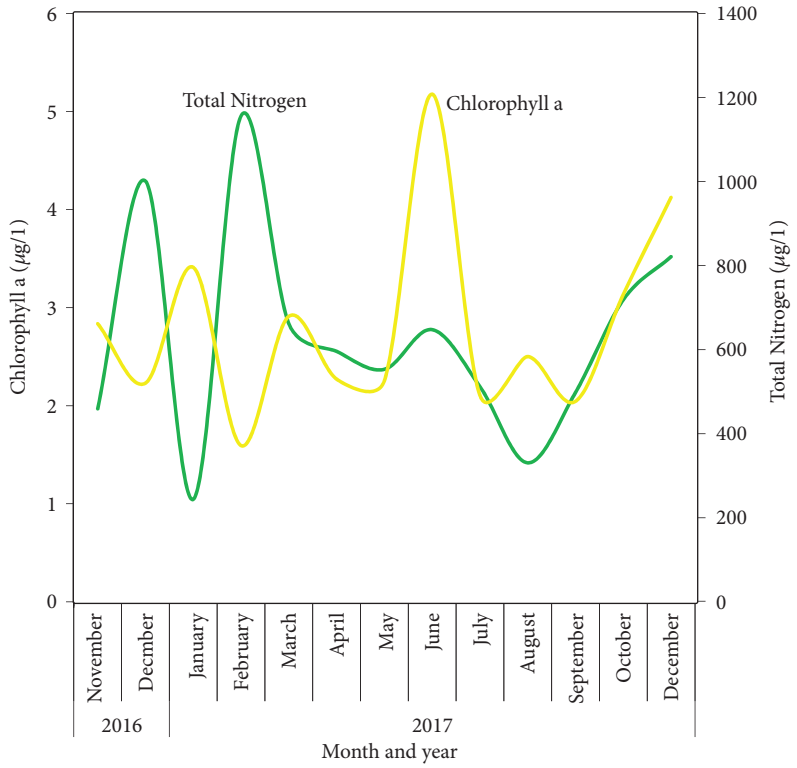

(a)

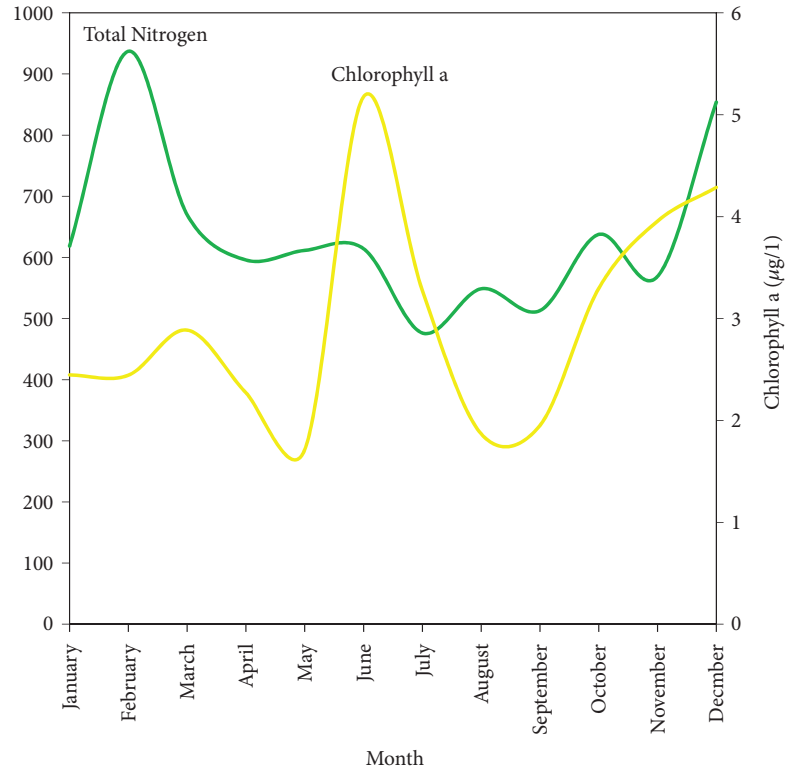

(b)

Figure 1: Continued.

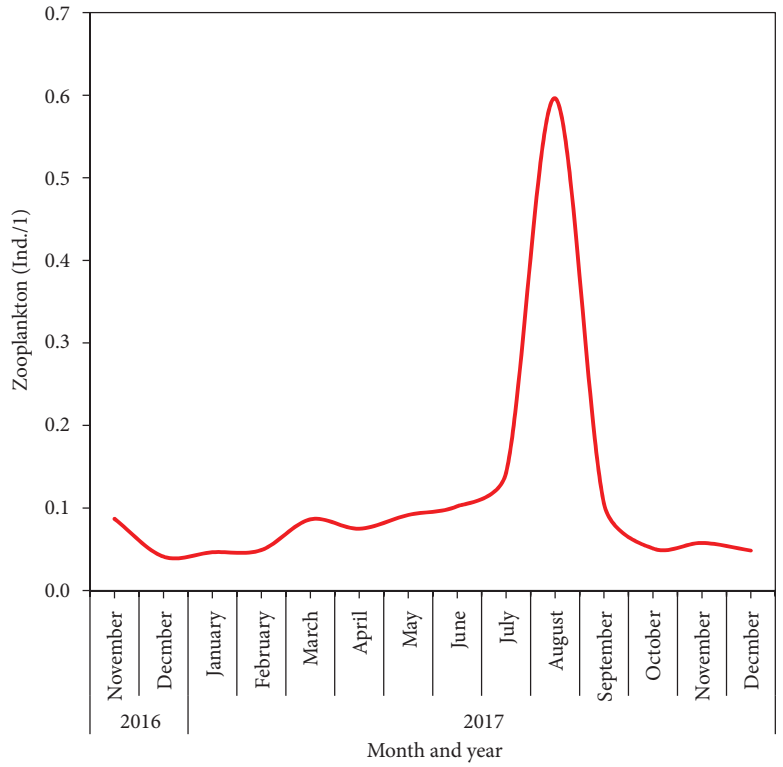

(c)

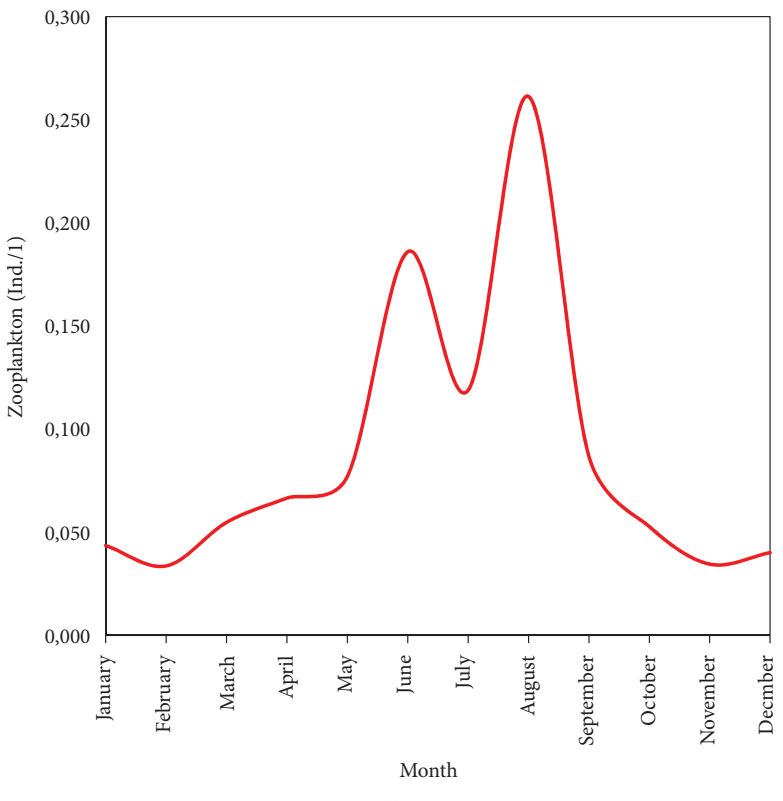

(d)

Figure 1: (a) Time series plot of total nitrogen and chlorophyll a; (b) a plot of monthly averages of total nitrogen and chlorophyll a; (c) time series plot of zooplankton; (d) a plot of monthly averages of zooplankton.

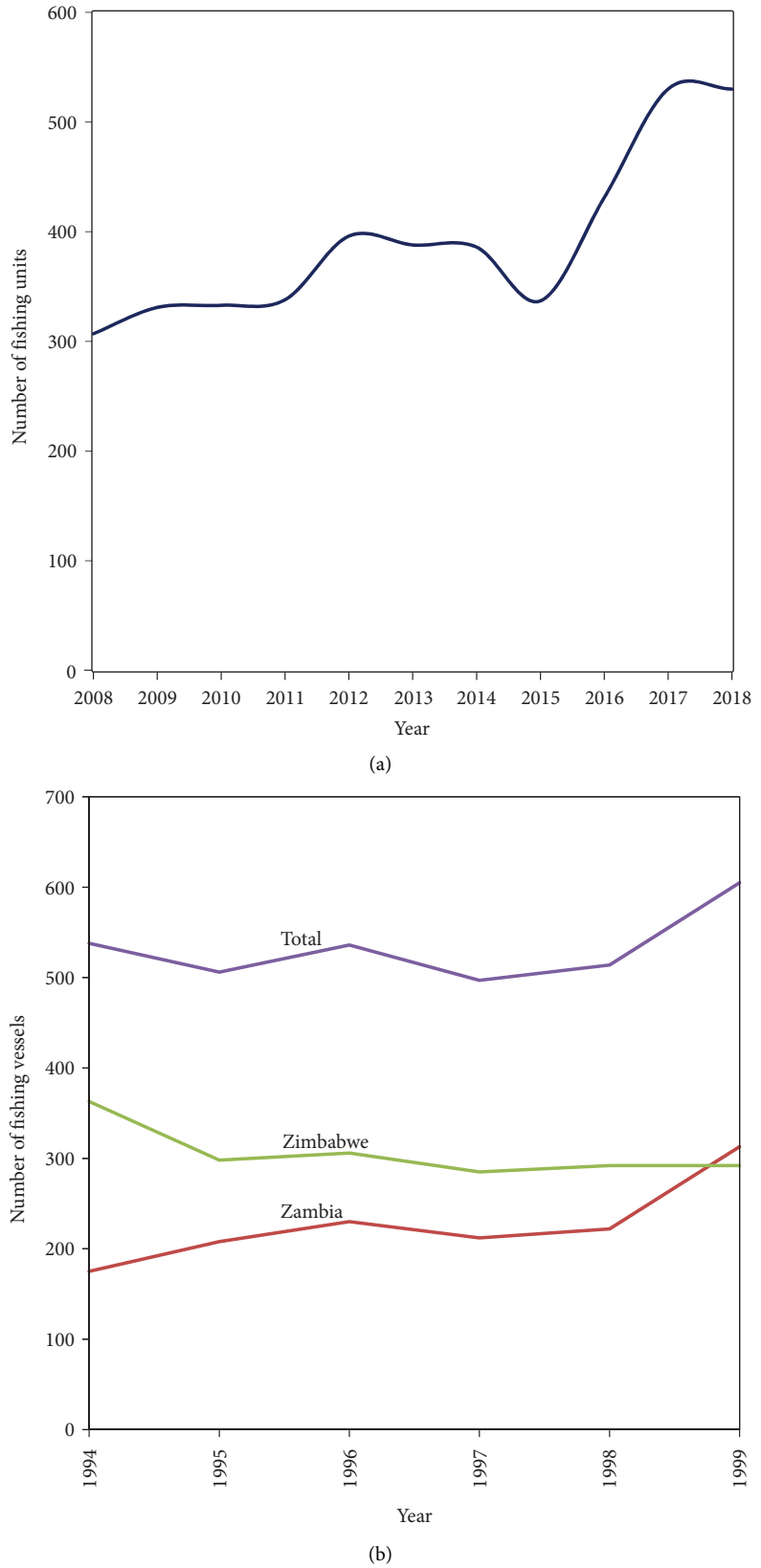

Figure 2: (a) Time series plot of fishing units from 2008 to 2018. (b) Time series plot of fishing units from 1994 to 1999 [27].

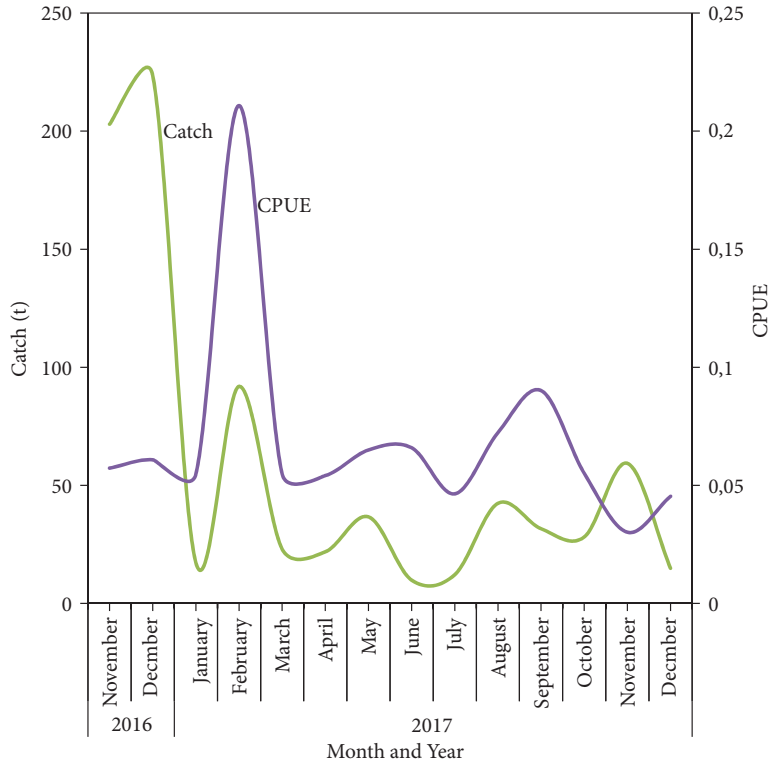

(a)

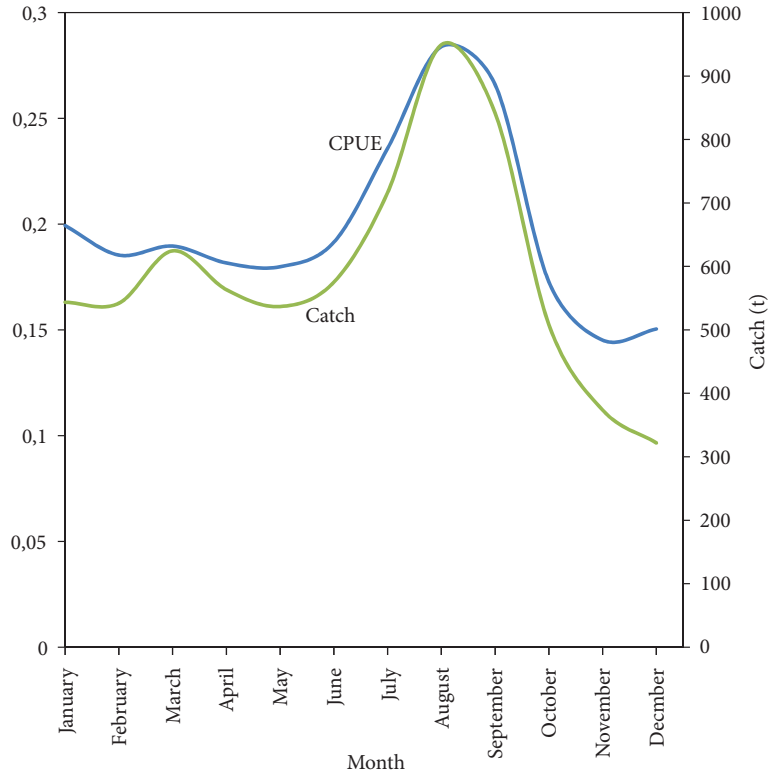

(b)

Figure 3: Continued.

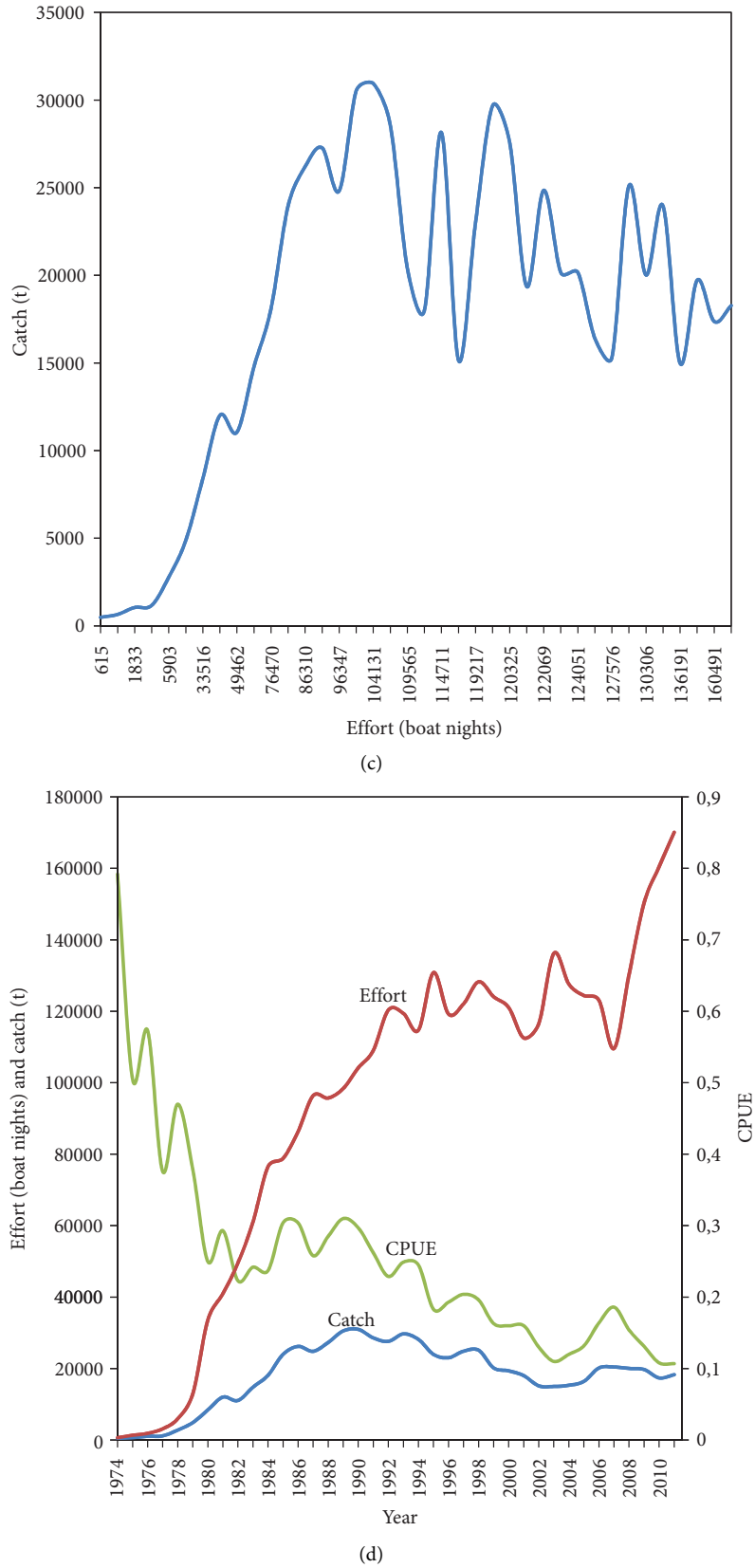

Figure 3: (a) Kapenta catch and CPUE time series plot; (b) a plot of monthly averages of kapenta catch and CPUE; (c) kapenta catch in Lake Kariba time series plot; (d) a plot of effort and CPUE in Lake Kariba.

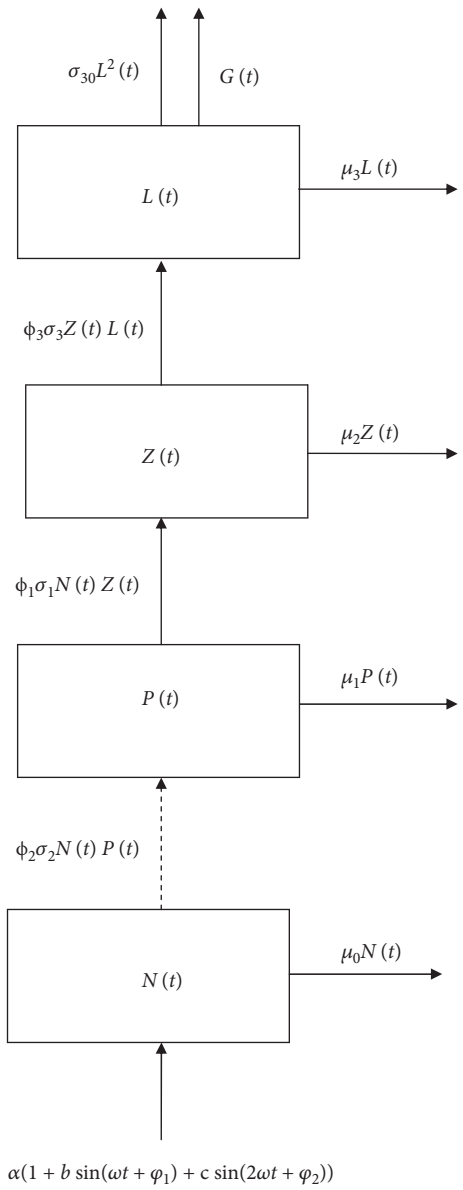

Figure 4: Flow diagram of the Limnothrissa miodon model with harvesting.

The nonlinear nonautonomous dynamical system with Schaefer harvesting is

$$\begin{aligned}
\frac{dN}{dt} &= a\left(1 + b\,\sin\left(\omega t + \varphi_1\right) + c\,\sin\left(2\omega t + \varphi_2\right)\right) - \mu_0 N - \sigma_1 NP,\\
\frac{dP}{dt} &= \phi_1\sigma_1 NP - \mu_1 P - \sigma_2 PZ,\\
\frac{dZ}{dt} &= \phi_2\sigma_2 PZ - \mu_2 Z - \sigma_3 ZL,\\
\frac{dL}{dt} &= \phi_3\sigma_3 ZL - \mu_3 L - \sigma_{30}L^2 - qEL.
\end{aligned} \tag{2}$$

Model (2) initial condition is,

$$\begin{cases}
N(0) = \psi_1(0), P(0) = \psi_2(0),\\
Z(0) = \psi_3(0), L(0) = \psi_4(0),\\
\psi_i(0) > 0, \quad i = 1, 2, 3, 4,
\end{cases} \tag{3}$$

and the mathematically feasible region is defined as

$$\mathbf{\Omega} = \left\{(N, P, Z, L) \in \mathbb{R}^4 | N \geq 0, P \geq 0, Z \geq 0, L \geq 0\right\}. \tag{4}$$

The crowding of the Limnothrissa miodon population coefficient is $\sigma_{30} > 0$. The constants of proportionality σ_i $(i = 1, 2, 3)$ are positive and depletion rate coefficients are represented by μ_i $(i = 0, 1, 2, 3)$.

2.4. Positivity of Solutions. We prove that, for positive initial data for the model (2), the solutions will remain positive $\forall t \geq 0$.

Theorem 1. *Let $N(t) \geq 0, P(t) \geq 0, Z(t) \geq 0, L(t) \geq 0$ be the initial data. Then, solutions of $N(t)$, $P(t)$, $Z(t)$, $L(t)$ of model (2) are positive $\forall t \geq 0$.*

Proof. Based on the first equation of system (2) and $N(t) \in [0, T]$, it follows that

$$\dot{N}(t) \geq -\mu_0 N(t) - \sigma_1 N(t) P(t), \quad \forall t \in [0, T]. \tag{5}$$

Consequently, we obtain

$$N(t) \geq N(0)\exp\int_0^t \left(-\mu_0 - \sigma_1 P(s)\right)ds \geq 0, \quad \forall t \in [0, T]. \tag{6}$$

According to the second equation of system (2),

$$\dot{P}(t) \geq -\mu_1 P(t) - \sigma_2 P(t) Z(t), \quad \forall t \in [0, T]. \tag{7}$$

The direct integration of (7) yields

$$P(t) \geq P(0)\exp\int_0^t \left(-\mu_1 - \sigma_2 Z(s)ds\right) \geq 0, \quad \forall t \in [0, T]. \tag{8}$$

According to the third equation of system (2),

$$\dot{Z}(t) \geq -\mu_2 Z(t) - \sigma_3 Z(t) L(t), \quad \forall t \in [0, T]. \tag{9}$$

The direct integration of (9) yields

$$Z(t) \geq Z(0)\exp\int_0^t \left(-\mu_2 - \sigma_3 L(s)\right)ds \geq 0, \quad \forall t \in [0, T]. \tag{10}$$

Considering the variable $L(t) \in [0, T]$, it follows from the fourth equation of system (2) that

$$\dot{L}(t) \geq -L(t)\left(\mu_3 + qE + \sigma_{30} L(t)\right), \quad \forall t \in [0, T]. \tag{11}$$

The direct integration of (11) yields

$$L(t) \geq \frac{(\mu_3 + qE) L(0) e^{-(\mu_3 + qE)t}}{\mu_3 + qE + \sigma_{30} L(0)\left(1 - e^{-(\mu_3 + qE)t}\right)} \geq 0, \quad \forall t \in [0, T]. \tag{12}$$

As a result, system solutions of (2) with initial conditions (3) remain positive $\forall t \geq 0$. □

2.5. Existence of Solutions

Theorem 2. *A solution of system (2) is feasible.*

Proof. We show that all feasible solutions of system (2) are uniformly bounded in $\Omega \subset \mathbb{R}^4$. Let any solution of system (2) be $\{(N(t), P(t), Z(t), L(t)) \in \mathbb{R}^4\}$, with nonnegative initial conditions.

Let $C(t) = N(t) + P(t) + Z(t) + L(t)$, and then

$$\begin{aligned}
\frac{dC}{dt} &= a\left(1 + b\,\sin(\omega t + \varphi_1) + c\,\sin(2\omega t + \varphi_2)\right) - \mu_0 N - \sigma_1 NP + \phi_1\sigma_1 NP - \mu_1 P - \sigma_2 PZ + \phi_2\sigma_2 PZ \\
&\quad - \mu_2 Z - \sigma_3 ZL + \phi_3\sigma_3 ZL - \mu_3 L - \sigma_{30} L^2 - qEL, \\
&= a\left(1 + b\,\sin(\omega t + \varphi_1) + c\,\sin(2\omega t + \varphi_2)\right) - \mu_0 N - \mu_1 P - \mu_2 Z - (\mu_3 + qE)L - \sigma_{30} L^2 \\
&\quad + \sigma_1(\phi_1 - 1)NP + \sigma_2(\phi_2 - 1)PZ + \sigma_3(\phi_3 - 1)ZL, \\
&\leq a\left(1 + b\,\sin(\omega t + \varphi_1) + c\,\sin(2\omega t + \varphi_2)\right) - \mu_0 N - \mu_1 P - \mu_2 Z - (\mu_3 + qE)L, \\
&\leq a\left(1 + b\,\sin(\omega t + \varphi_1) + c\,\sin(2\omega t + \varphi_2)\right) - mC(t),
\end{aligned} \tag{13}$$

where $m = \min\{(\mu_0, \mu_1, \mu_2, \mu_3 + qE)\}$. Thus,

$$\frac{dC(t)}{dt} + mC(t) \leq a\left(1 + b\,\sin(\omega t + \varphi_1) + c\,\sin(2\omega t + \varphi_2)\right). \tag{14}$$

Equation (14) is a first-order differential inequality, with the solution given by

$$\begin{aligned}
0 < C(N, P, Z, L) \leq{}& \frac{a\left(bm^4 \sin(t\omega + \varphi_1) + 4bm^2\omega^2 \sin(t\omega + \varphi_1) + cm^4 \sin(2t\omega + \varphi_2) + cm^2\omega^2 \sin(2t\omega + \varphi_2)\right)}{m^5 + 5m^3\omega^2 + 4m\omega^4} \\
&- \frac{a\left(bm\omega\left(m^2 + 4\omega^2\right)\cos(t\omega + \varphi_1) + 2cm\omega\left(m^2 + \omega^2\right)\cos(2t\omega + \varphi_2) + m^4 + 5m^2\omega^2 + 4\omega^4\right)}{m^5 + 5m^3\omega^2 + 4m\omega^4} + C_0 e^{-mt},
\end{aligned} \tag{15}$$

as $t \longrightarrow \infty$, (15) becomes

$$\begin{aligned}
0 < C(N, P, Z, L) \leq{}& \frac{a\left(bm^4 \sin(t\omega + \varphi_1) + 4bm^2\omega^2 \sin(t\omega + \varphi_1) + cm^4 \sin(2t\omega + \varphi_2) + cm^2\omega^2 \sin(2t\omega + \varphi_2)\right)}{m^5 + 5m^3\omega^2 + 4m\omega^4} \\
&- \frac{a\left(bm\omega\left(m^2 + 4\omega^2\right)\cos(t\omega + \varphi_1) + 2cm\omega\left(m^2 + \omega^2\right)\cos(2t\omega + \varphi_2) + m^4 + 5m^2\omega^2 + 4\omega^4\right)}{m^5 + 5m^3\omega^2 + 4m\omega^4}.
\end{aligned} \tag{16}$$

Therefore, all solutions of system (2) enter the feasible region,

$$\Omega = \Big\{(N(t), P(t), Z(t), L(t)) \in \mathbb{R}_+^4 : C \leq \frac{a\left(bm^4 \sin(t\omega + \varphi_1) + 4bm^2\omega^2 \sin(t\omega + \varphi_1) + cm^4 \sin(2t\omega + \varphi_2) + cm^2\omega^2 \sin(2t\omega + \varphi_2)\right)}{m^5 + 5m^3\omega^2 + 4m\omega^4} - \frac{a\left(bm\omega\left(m^2 + 4\omega^2\right)\cos(t\omega + \varphi_1) + 2cm\omega\left(m^2 + \omega^2\right)\cos(2t\omega + \varphi_2) + m^4 + 5m^2\omega^2 + 4\omega^4\right)}{m^5 + 5m^3\omega^2 + 4m\omega^4} + \varsigma, \forall \varsigma > 0\Big\}. \tag{17}$$

This concludes the theorem's proof. □

2.6. Equilibrium States for the Autonomous Model. Of biological interest is the coexistence equilibrium. If $b = c = 0$ in system (2), then the model is autonomous and has a unique coexistence equilibrium, $\mathscr{E}_* = (N^*, P^*, Z^*, L^*)$, which is obtained through the solution of the equations:

$$a - \mu_0 N - \sigma_1 NP = 0, \tag{18}$$

$$\phi_1\sigma_1 N - \mu_1 - \sigma_2 Z = 0, \tag{19}$$

$$\phi_2\sigma_2 P - \mu_2 - \sigma_3 L = 0, \tag{20}$$

$$\phi_3\sigma_3 Z - \mu_3 - qE - \sigma_{30} L = 0. \tag{21}$$

Solving for N, P, Z, and L in (18)–(21) gives

$$\sigma_1\sigma_2\sigma_3\sigma_{30}(L^*)^2 + \left(\sigma_1\sigma_2\sigma_3(\mu_3 + qE) + \sigma_1\sigma_2\mu_2\sigma_{30} + \mu_0\sigma_2^2\phi_2\sigma_{30} + \mu_1\sigma_1\sigma_3^2\phi_3\right)L^* + \mu_0\mu_1\phi_2\sigma_2\phi_3\sigma_3 + \mu_1\sigma_1\mu_2\phi_3\sigma_3 + \mu_0\sigma_2^2\phi_2(\mu_3 + qE) + \sigma_1\sigma_2\mu_2(\mu_3 + qE) - a\phi_1\sigma_1\phi_2\sigma_2\phi_3\sigma_3 = 0. \tag{22}$$

If expression (24) is positive, (23) will have a unique positive root:

$$L^* = \frac{\sqrt{A_1^2 - 4\sigma_1\sigma_2\sigma_3\sigma_{30}A_2} - A_1}{2\sigma_1\sigma_2\sigma_3\sigma_{30}} > 0, \tag{23}$$

where

$$A_1 = \sigma_1\sigma_2\sigma_3(\mu_3 + qE) + \sigma_1\sigma_2\mu_2\sigma_{30} + \mu_0\sigma_2^2\phi_2\sigma_{30} + \mu_1\sigma_1\sigma_3^2\phi_3,$$
$$A_2 = \mu_0\mu_1\phi_2\sigma_2\phi_3\sigma_3 + \mu_1\sigma_1\mu_2\phi_3\sigma_3 + \mu_0\sigma_2^2\phi_2(\mu_3 + qE) + \sigma_1\sigma_2\mu_2(\mu_3 + qE) - a\phi_1\sigma_1\phi_2\sigma_2\phi_3\sigma_3. \tag{24}$$

And (23) can be written as

$$A_1^2 - 4\sigma_1\sigma_2\sigma_3\sigma_{30}A_2 > A_1^2,$$
$$\sigma_1\sigma_2\sigma_3\sigma_{30}A_2 < 0,$$
$$(\sigma_1\sigma_2\sigma_3\sigma_{30})\left(\mu_0\mu_1\phi_2\sigma_2\phi_3\sigma_3 + \mu_1\sigma_1\mu_2\phi_3\sigma_3 + \mu_0\sigma_2^2\phi_2(\mu_3 + qE) + \sigma_1\sigma_2\mu_2(\mu_3 + qE) - a\phi_1\sigma_1\phi_2\sigma_2\phi_3\sigma_3\right) < 0, \tag{25}$$
$$\sigma_2(\mu_3 + qE)(\mu_0\sigma_2\phi_2 + \sigma_1\mu_2) < \phi_3\sigma_3(a\phi_1\sigma_1\phi_2\sigma_2 - (\mu_0\mu_1\phi_2\sigma_2 + \mu_1\mu_2\sigma_1)),$$
$$\frac{\mu_3 + qE}{\phi_3\sigma_3} < \frac{a\phi_1\sigma_1\phi_2\sigma_2 - (\mu_0\mu_1\phi_2\sigma_2 + \mu_1\mu_2\sigma_1)}{\sigma_2(\mu_0\sigma_2\phi_2 + \sigma_1\mu_2)}.$$

Therefore, L^* exists whenever

$$\frac{a\phi_1\sigma_1\phi_2\sigma_2 - (\mu_0\mu_1\phi_2\sigma_2 + \mu_1\mu_2\sigma_1)}{\sigma_2(\mu_0\sigma_2\phi_2 + \sigma_1\mu_2)} > \frac{\mu_3 + qE}{\phi_3\sigma_3}. \tag{26}$$

The equilibrium $\mathscr{E}_*$ is

$$\begin{aligned}
N^* &= \frac{\sigma_1\sigma_2\sigma_3(\mu_3 + qE) - \mu_2\sigma_1\sigma_2\sigma_{30} - \mu_0\sigma_2^2\sigma_{30}\phi_2 + \mu_1\sigma_1\sigma_3^2\phi_3 + \sqrt{4A_3 + A_4^2}}{2\sigma_1^2\sigma_3^2\phi_1\phi_3},\\
P^* &= \frac{-\sigma_1\sigma_2\sigma_3(\mu_3 + qE) + \mu_2\sigma_1\sigma_2\sigma_{30} - \mu_0\sigma_2^2\sigma_{30}\phi_2 - \mu_1\sigma_1\sigma_3^2\phi_3 + \sqrt{4A_3 + A_4^2}}{2\sigma_1\sigma_2^2\sigma_{30}\phi_2},\\
Z^* &= \frac{\sigma_1\sigma_2\sigma_3(\mu_3 + qE) - \mu_2\sigma_1\sigma_2\sigma_{30} - \mu_0\sigma_2^2\sigma_{30}\phi_2 - \mu_1\sigma_1\sigma_3^2\phi_3 + \sqrt{4A_3 + A_4^2}}{2\sigma_1\sigma_2\sigma_3^2\phi_3},\\
L^* &= \frac{-\sigma_1\sigma_2\sigma_3(\mu_3 + qE) - \mu_2\sigma_1\sigma_2\sigma_{30} - \mu_0\sigma_2^2\sigma_{30}\phi_2 - \mu_1\sigma_1\sigma_3^2\phi_3 + \sqrt{4A_3 + A_4^2}}{2\sigma_1\sigma_2\sigma_3\sigma_{30}},
\end{aligned} \tag{27}$$

where

$$\begin{aligned}
A_3 &= a\sigma_1^2\sigma_2^2\sigma_3^2\sigma_{30}\phi_1\phi_2\phi_3,\\
A_4 &= \sigma_1\sigma_2\sigma_3(\mu_3 + qE) - \sigma_2\sigma_{30}(\mu_2\sigma_1 + \mu_0\sigma_2\phi_2) + \mu_1\sigma_1\sigma_3^2\phi_3.
\end{aligned} \tag{28}$$

From equation array (27), it follows that

$$\begin{aligned}
N^* &= \frac{\sigma_1\sigma_2\sigma_3(\mu_3 + qE) - \mu_2\sigma_1\sigma_2\sigma_{30} - \mu_0\sigma_2^2\sigma_{30}\phi_2 + \mu_1\sigma_1\sigma_3^2\phi_3 + \sqrt{4A_3 + A_4^2}}{2\sigma_1^2\sigma_3^2\phi_1\phi_3},\\
P^* &= \frac{\sigma_1\sigma_3^2\phi_1\phi_3N^* - \sigma_2\sigma_3(\mu_3 + qE) + \mu_2\sigma_2\sigma_{30} - \mu_1\sigma_3^2\phi_3}{\sigma_2^2\sigma_{30}\phi_2},\\
Z^* &= \frac{\sigma_2\sigma_{30}\phi_2P^* + \sigma_3(\mu_3 + qE) - \mu_2\sigma_{30}}{\sigma_3^2\phi_3},\\
L^* &= \frac{\sigma_3\phi_3Z^* - (\mu_3 + qE)}{\sigma_{30}}.
\end{aligned} \tag{29}$$

The coexistence equilibrium, $\mathscr{E}_* = (0.134444, 503.68, 0.0694424, 128.578)$, for the autonomous model (2), with damped oscillations for the set of default parameters $a = 618.8$, $\mu_0 = 0.2924$, $\sigma_1 = 9.13751$, $\phi_1 = 1$, $\mu_1 = 0.974667$, $\sigma_2 = 3.655$, $\phi_2 = 1$, $\mu_2 = 0.30458$, $\sigma_3 = 14.31542$, $\sigma_{30} = 0.000152$, $\phi_3 = 1$, $\mu_3 = 0.834558$, $q = 0.00000918$, and $E = 15250$, are shown in Figure 5.

2.7. Stability Analysis for the Autonomous Model. If $b = c = 0$ in system (2), then the model has a unique coexistence equilibrium $\mathscr{E}_*$ which is locally stable.

Theorem 3. *If the equilibrium $\mathscr{E}_*$ exists, then it is locally asymptotically stable if the conditions in (39) are met.*

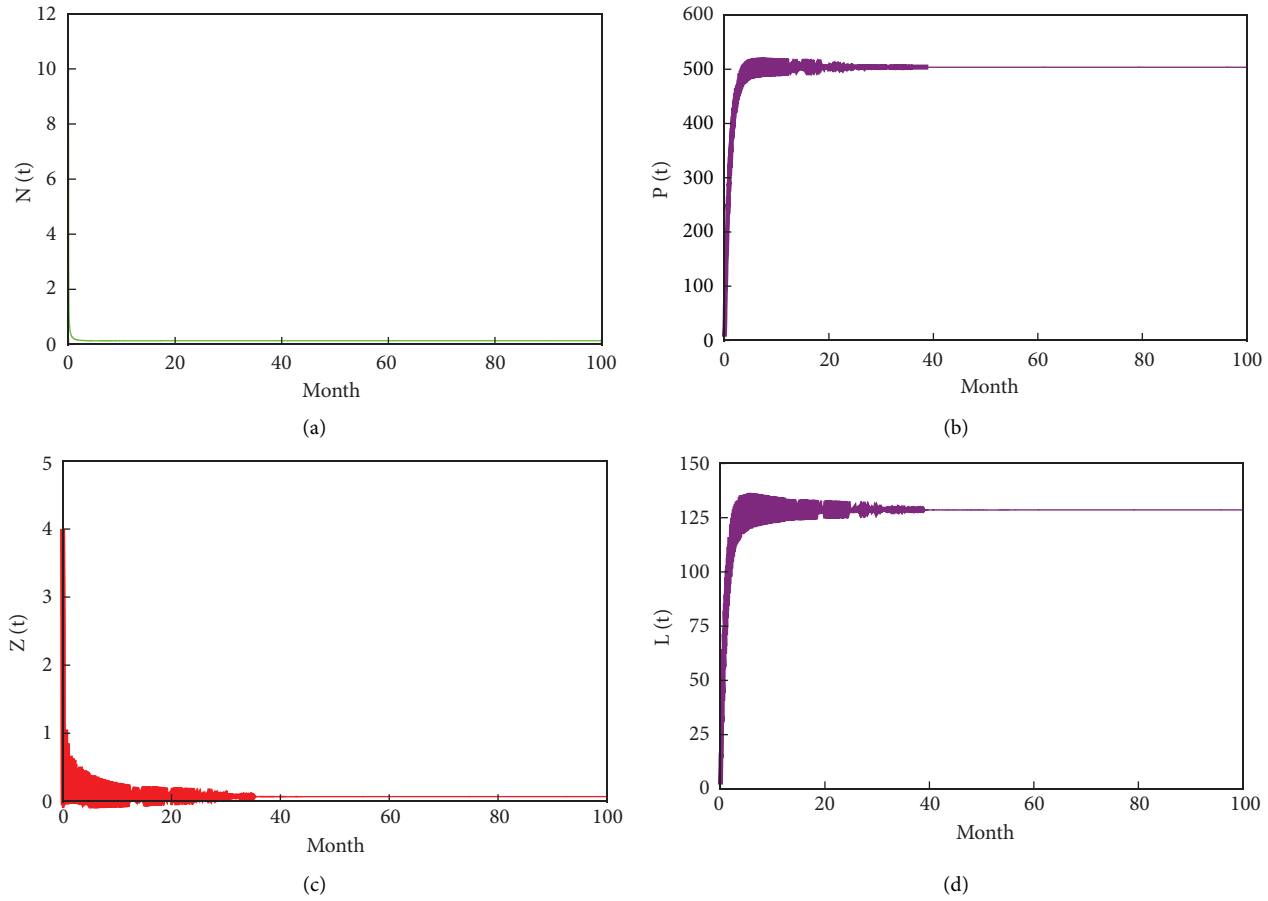

FIGURE 5: Time series plot of (a) nutrients; (b) phytoplankton; (c) zooplankton; (d) Limnothrissa miodon for system (2) for model (2) with $b = c = 0$ and assumed initial condition: $N(0) = 10, P(0) = 7, Z(0) = 4, L(0) = 2$ using the default parameter values.

Proof. The stability of the equilibrium states of model (2) are determined by the Jacobian matrix [30], $\mathcal{J}$, of system (2):

$$\mathcal{J} = \begin{pmatrix} -\mu_0 - \sigma_1 P & -\sigma_1 N & 0 & 0 \\ \phi_1\sigma_1 P & \phi_1\sigma_1 N - \mu_1 - \sigma_2 Z & -\sigma_2 P & 0 \\ 0 & \phi_2\sigma_2 Z & \phi_2\sigma_2 P - \mu_2 - \sigma_3 L & -\sigma_3 Z \\ 0 & 0 & \phi_3\sigma_3 L & \phi_3\sigma_3 Z - \mu_3 - qE - 2\sigma_{30} L \end{pmatrix}. \tag{30}$$

Evaluating $\mathcal{J}$ at $\mathcal{E}_*$ results in

$$\mathcal{J}_{\mathcal{E}_*} = \begin{pmatrix} -\mu_0 - \sigma_1 c_5 & -\sigma_1 c_4 & 0 & 0 \\ \phi_1\sigma_1 c_5 & \phi_1\sigma_1 c_4 - \mu_1 - \sigma_2 c_6 & -\sigma_2 c_5 & 0 \\ 0 & \phi_2\sigma_2 c_6 & \phi_2\sigma_2 c_5 - \mu_2 - \sigma_3 c_7 & -\sigma_3 c_6 \\ 0 & 0 & \phi_3\sigma_3 c_7 & \phi_3\sigma_3 c_6 - \mu_3 - qE - 2\sigma_{30} c_7 \end{pmatrix}, \tag{31}$$

where $c_4 = N^*$, $c_5 = P^*$, $c_6 = Z^*$, and $c_7 = L^*$. Then, (31) simplifies to

$$\mathcal{J}_{\mathscr{E}_*} = \begin{pmatrix} -\mu_0 - \sigma_1 c_5 & -\sigma_1 c_4 & 0 & 0 \\ \phi_1 \sigma_1 c_5 & 0 & -\sigma_2 c_5 & 0 \\ 0 & \phi_2 \sigma_2 c_6 & 0 & -\sigma_3 c_6 \\ 0 & 0 & \phi_3 \sigma_3 c_7 & \phi_3 \sigma_3 c_6 - \mu_3 - qE - 2\sigma_{30} c_7 \end{pmatrix}. \tag{32}$$

The eigenvalues of (32) are the roots of the auxiliary equation

$$\begin{aligned} \Delta(\lambda) = {} & c_6 c_7 \sigma_3^2 \left(\lambda^2 + \lambda\mu_0 + c_5\sigma_1(\lambda + c_4\sigma_1\phi_1)\right)\phi_3 + \left(\lambda\left(\lambda^2 + \lambda\mu_0 + c_5\sigma_1(\lambda + c_4\sigma_1\phi_1)\right)\right. \\ & \left. + c_5 c_6 (\lambda + \mu_0 + c_5\sigma_1)\sigma^2\phi_2\right)(\lambda + \mu_3 + qE + 2c_7\sigma_{30} - c_6\sigma_3\phi_3) = 0. \end{aligned} \tag{33}$$

The auxiliary (33) can be expressed as follows:

$$\Delta(\lambda) = \lambda^4 + a_1\lambda^3 + a_2\lambda^2 + a_3\lambda + a_4 = 0, \tag{34}$$

where

$$\begin{aligned} a_1 &= \mu_0 + \mu_3 + qE + c_5\sigma_1 + 2c_7\sigma_{30} - c_6\sigma_3\phi_3, \\ a_2 &= c_5 qE\sigma_1 - c_6\mu_0\sigma_3\phi_3 + c_5\mu_3\sigma_1 + 2c_7\mu_0\sigma_{30} + c_4 c_5\sigma_1^2\phi_1 - c_5 c_6\sigma_3\sigma_1\phi_3 \\ &\quad + c_5 c_6\sigma_2^2\phi_2 + c_6 c_7\sigma_3^2\phi_3 + 2c_5 c_7\sigma_{30}\sigma_1 + qE\mu_0 + \mu_0\mu_3, \\ a_3 &= c_4 c_5\sigma_1^2\phi_1(-c_6\sigma_3\phi_3 + 2c_7\sigma_{30} + qE + \mu_3) + c_6\left(c_5\left(\sigma_2^2\phi_2(-c_6\sigma_3\phi_3 + 2c_7\sigma_{30} + qE + \mu_0 + \mu_3)\right)\right) \\ &\quad + c_7\sigma_1\sigma_3^2\phi_3\Big) + c_7\mu_0\sigma_3^2\phi_3 + c_5^2\sigma_1\sigma_2^2\phi_2\Big), \\ a_4 &= c_5 c_6 qE\mu_0\sigma_2^2\phi_2 + c_5^2 c_6 qE\sigma_1\sigma_2^2\phi_2 + c_5 c_6\mu_0\mu_3\sigma_2^2\phi_2 + c_5^2 c_6\mu_3\sigma_1\sigma_2^2\phi_2 + 2c_5 c_6 c_7\mu_0\sigma_{30}\sigma_2^2\phi_2 \\ &\quad - c_5 c_6^2\mu_0\sigma_3\sigma_2^2\phi_2\phi_3 + 2c_5^2 c_6 c_7\sigma_1\sigma_{30}\sigma_2^2\phi_2 - c_5^2 c_6^2\sigma_1\sigma_3\sigma_2^2\phi_2\phi_3 + c_4 c_5 c_6 c_7\sigma_1^2\sigma_3^2\phi_1\phi_3. \end{aligned} \tag{35}$$

According to the Routh–Hurwitz criterion, all eigenvalues of the auxiliary (34) have negative real parts if

$$a_1 > 0, a_1 a_2 - a_3 > 0, a_3(a_1 a_2 - a_3) - a_1^2 a_4 > 0, a_4 > 0. \tag{36}$$

□

Remark 1. If the conditions $b = c = 0$ for $\mathscr{E}_*$ are not satisfied for a given set of parameter values, then the respective steady state has a possibility of oscillatory behaviour for model (2).

Theorem 4. *If the conditions in (42) for the Lyapunov function in (40) are met, the equilibrium $\mathscr{E}_*$ is globally asymptotically stable.*

Proof. The proof is based on Lyapunov's second method. Let $N - N^* > 0$, $P - P^* > 0$, $Z - Z^* > 0$, $L - L^* > 0$. Let $V(N, P, Z, L)$ be a positive definite Lyapunov function [31] such that $V(N^*, P^*, Z^*, L^*) = 0$ by

$$\begin{aligned} V(N, P, Z, L) = {} & \xi_1\left(N - N^* - N^*\ln\frac{N}{N^*}\right) + \xi_2\left(P - P^* - P^*\ln\frac{P}{P^*}\right) \\ & + \xi_3\left(Z - Z^* - Z^*\ln\frac{Z}{Z^*}\right) + \xi_4\left(L - L^* - L^*\ln\frac{L}{L^*}\right), \end{aligned} \tag{37}$$

where $\xi_i's$, $i = 1, 2, 3, 4$, are positive constants. V is a positive definite function in the set Ψ, except at $\mathscr{E}_*$ where it is zero. The derivative of V with respect to solution of system (2) is

$$\begin{aligned}\dot{V} &= \xi_1(N - N^*)\frac{\dot{N}}{N} + \xi_2(P - P^*)\frac{\dot{P}}{P} + \xi_3(Z - Z^*)\frac{\dot{Z}}{Z} + \xi_4(L - L^*)\frac{\dot{L}}{L},\\ &= -\xi_1(N - N^*)\left[\mu_0 + \sigma_1 P - \frac{a}{N}\right] - \xi_2(P - P^*)[\mu_1 + \sigma_2 Z - \phi_1\sigma_1 N]\\ &\quad - \xi_3(Z - Z^*)[\mu_2 + \sigma_3 L - \phi_2\sigma_2 P] - \xi_4(L - L^*)[\mu_3 + qE + \sigma_{30}L - \phi_3\sigma_3 Z].\end{aligned} \tag{38}$$

Then $\dot{V} < 0$ if

$$\begin{aligned}&\mu_0 + \sigma_1 P > \frac{a}{N},\\ &\mu_1 + \sigma_2 Z > \phi_1\sigma_1 N,\\ &\mu_2 + \sigma_3 L > \phi_2\sigma_2 P,\ \mu_3 + qE + \sigma_{30}L > \phi_3\sigma_3 Z.\end{aligned} \tag{39}$$

Thus, $\mathscr{E}_*$ is globally asymptotically stable in the region bounded by all points $(N > N^*,\ P > P^*,\ Z > Z^*,\ L > L^*)$ in (39). □

2.7.1. Fishing Effort. From model (2),

$$\frac{dL}{dt} = \phi_3\sigma_3 ZL - \mu_3 L - \sigma_{30}L^2 - qEL. \tag{40}$$

For the autonomous model (2), (43) at equilibrium is

$$qEL^* = \phi_3\sigma_3 Z^* L^* - \mu_3 L^* - \sigma_{30}L^{*(2)}. \tag{41}$$

We let

$$h = \phi_3\sigma_3 Z^* L^* - \mu_3 L^* - \sigma_{30}L^{*(2)}, \tag{42}$$

and $\partial h/\partial L^* = 0$ yields

$$\phi_3\sigma_3 Z^* - \mu_3 - 2\sigma_{30}L^* = 0, \tag{43}$$

and $\therefore$

$$h = qE\left(\frac{\phi_3\sigma_3 Z^* - \mu_3 - qE}{2\sigma_{30}}\right), \tag{44}$$

and $\partial^2 h/\partial L^{*(2)} < 0$ meaning h is the maximum sustainable catch. For sustainability of the kapenta resource, the sustainable fishing effort is

$$qE < \phi_3\sigma_3 Z^* - \mu_3. \tag{45}$$

For the autonomous system, at equilibrium, the kapenta catch is

$$h = qeL^* = 0.00000918 \times 15250 \times 128.578 = 18.00027711\ \mu\text{gl}^{-1}, \tag{46}$$

and it is shown in Figure 6. The surface (colour green) is for the equation $h = \phi_3\sigma_3 Z^* L^* - \mu_3 L^* - \sigma_{30}L^{*(2)}$ and the surface (colour magenta) is for the equation $h = qEL^*$.

Assuming the lake is at its capacity of 160 km^3 and a carrying capacity of 240500 tonnes obtained by Tendaupenyu and Pyo [17], 18.00027711 μgl^{-1} of Limnothrissa miodon is an average monthly catch of 2889.05 tonnes and an average yearly total of 34668.59 tonnes. From (43),

$$L^* = \frac{\phi_3\sigma_3 Z^* - \mu_3}{2\sigma_{30}}. \tag{47}$$

The maximum sustainable catch, h, can be written as

$$h = \frac{1}{4\sigma_{30}}(\phi_3\sigma_3 Z^* - \mu_3)^2. \tag{48}$$

h is a function of the variables in the food chain and parameters and this result is a true reflection of what happens in the lake as a result of the environmental factors which are not constant. The maximum sustainable catch of 34668.59 t is within the range of the MSY of 25372 t obtained by Tendaupenyu and Pyo [17] and MSY of 40000 t obtained by Magadza [14].

2.8. Optimal Harvesting for the Autonomous Model. For model (2) with $b = c = 0$, we formulate a Hamiltonian function and apply Pontryagin's maximum principle [32].

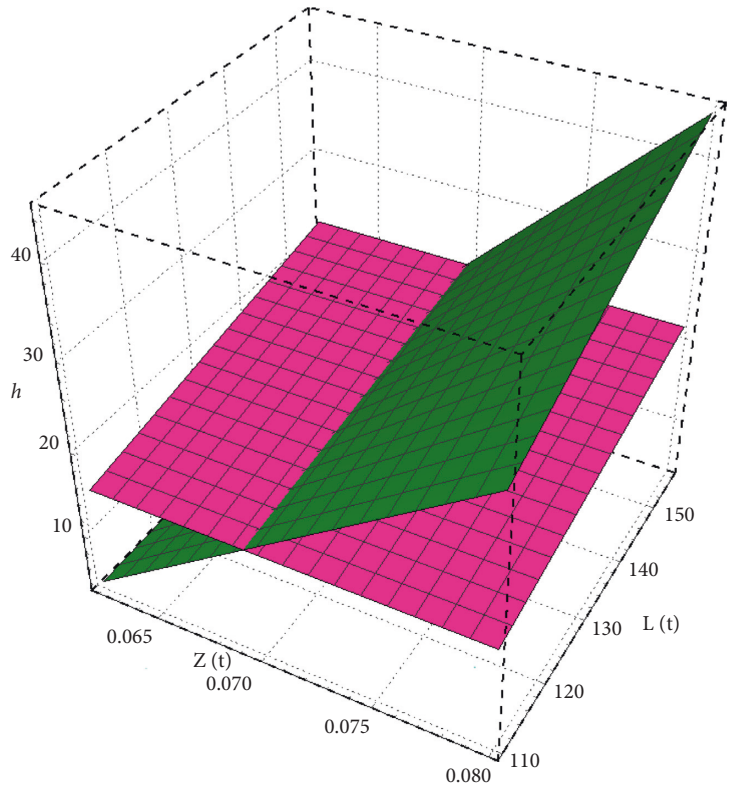

FIGURE 6: Plot of catch, $Z(t)$ and $L(t)$ at steady state.

$$\text{The optima sustainable yield (OSY)} = \text{total revenue (TR)} - \text{total cost (TC)}, \tag{49}$$

where TR and TC are the total revenue from selling harvested kapenta and the total cost of harvesting the kapenta, respectively. For the harvesting function, $h = qEL$,

$$\text{OSY} = (\alpha qL - \beta)E. \tag{50}$$

Then,

$$J = \int_0^{\infty} e^{-\delta t}(\alpha qL - \beta)E(t)\mathrm{d}t \tag{51}$$

is a continuous time inflow of revenue, α is the price per unit of harvested kapenta, β is the utilised cost per unit effort, and δ is annual discount rate in the price of kapenta. Our goal is to maximize J subject to the equations in (18)–(21) and given the control constraints $0 < E < E_{\max}$. To determine the optimal level of equilibrium, we employ Pontryagin's maximum principle [32]. For the autonomous model (2) and (54), the Hamiltonian function is

$$\begin{aligned} H = {} & e^{-\delta t}(\alpha qL - \beta)E + \lambda_1(t)\left(a - \mu_0 N - \sigma_1 NP\right) + \lambda_2(t)\left(\gamma_1 NP - \mu_1 P - \sigma_2 PZ\right) \\ & + \lambda_3(t)\left(\gamma_2 PZ - \mu_2 Z - \sigma_3 ZL\right) + \lambda_4(t)\left(\gamma_3 ZL - \mu_3 L - \sigma_{30}L^2 - qEL\right), \end{aligned} \tag{52}$$

where $\gamma_1 = \phi_1\sigma_1$, $\gamma_2 = \phi_2\sigma_2$, $\gamma_3 = \phi_3\sigma_3$, $\lambda_1, \lambda_2, \lambda_3$ and λ_4 are adjoint variables and

$$\sigma(t) = e^{-\delta t}\left(\alpha qL^2 - \beta\right) - \lambda_4\left(qL^2\right) \tag{53}$$

is a switching function [32]. The condition in (54) must be met by the optimal control E that maximises H,

$$E = \begin{cases} E_{\max}, & \sigma(t) > 0; \lambda_4 e^{\delta t} < \left(\alpha - \dfrac{\beta}{qL^2}\right), \\ 0, & \sigma(t) < 0; \lambda_4 e^{\delta t} > \left(\alpha - \dfrac{\beta}{qL^2}\right), \end{cases} \tag{54}$$

where $\alpha - \beta/qL^2$ is the net economic revenue from unit kapenta harvest and $\lambda_4 e^{\delta t}$ is the shadow price [32]. The optimal harvesting policy is

$$E = \begin{cases} E_{\max}, & \sigma(t) > 0, \\ 0, & \sigma(t) < 0, \\ E^*, & \sigma(t) = 0, \end{cases} \tag{55}$$

where $E = E_{\max}$ if the shadow price is less than the net economic revenue on a unit kapenta harvest, $E = 0$ if the shadow price is greater than the net economic revenue on a unit kapenta harvest, and $E = E^*$ when the shadow price equals the net economic revenue on a unit kapenta harvest [32]. If $\sigma(t) = 0$, then $\partial H/\partial E = 0$, indicating that H does not depend on E, the control variable, which is required for the singular control E^* to be optimal on the interval $0 < E^* < E_{\max}$ [32]. Substituting $\sigma(t)$ into (53),

$$\lambda_4 = e^{-\delta t}\left(\alpha - \frac{\beta}{qL^2}\right). \tag{56}$$

The adjoint equations are

$$\frac{d\lambda_1}{dt} = -\frac{\partial H}{\partial N}, \frac{d\lambda_2}{dt} = -\frac{\partial H}{\partial P}, \frac{d\lambda_3}{dt} = -\frac{\partial H}{\partial Z}, \frac{d\lambda_4}{dt} = -\frac{\partial H}{\partial L}. \tag{57}$$

From the equations in (60),

$$\begin{aligned} \frac{d\lambda_1}{dt} &= -\lambda_1(\mu_0 - \sigma_1 P) - \lambda_2\gamma_1 P, \\ \frac{d\lambda_2}{dt} &= -\lambda_1(-\sigma_1 N) - \lambda_2(\gamma_1 N - \mu_1 - \sigma_2 Z) - \lambda_3(\gamma_2 Z), \\ \frac{d\lambda_3}{dt} &= -\lambda_2(-\sigma_2 P) - \lambda_3(\gamma_2 P - \mu_2 - \sigma_3 L) - \lambda_4(\gamma_3 L), \\ \frac{d\lambda_4}{dt} &= -\lambda_3(-\sigma_3 Z) - \lambda_4(\gamma_3 Z - \mu_3 - 2\sigma_{30} L - qE) - \alpha q E e^{-\delta t}. \end{aligned} \tag{58}$$

From (56),

$$\frac{d\lambda_4}{dt} = -\delta\lambda_4. \tag{59}$$

Substituting $\sigma(t) = 0$ in (53), we obtain

$$\lambda_4 = \left(\alpha - \frac{\beta}{qL^2}\right)e^{-\delta t}. \tag{60}$$

From (59) and the last equation of (58),

$$-\delta\lambda_4 = -\lambda_3(-\sigma_3 Z) - \lambda_4(\gamma_3 Z - \mu_3 - 2\sigma_{30} L - qE) - \alpha q E e^{-\delta t}. \tag{61}$$

Substituting (60) into (61) results in

$$\lambda_3 = e^{-\delta t}\left[\frac{\left(\alpha - \left(\beta/qL^2\right)\right)(\gamma_3 Z - \mu_3 - 2\sigma_{30} L - qE - \delta) + \alpha q E}{\sigma_3 Z}\right]. \tag{62}$$

Substituting (21) into (62) results in

$$\lambda_3 = -e^{-\delta t}\left[\frac{\left(\alpha - \left(\beta/qL^2\right)\right)(\delta + \sigma_{30} L) - \alpha q E}{\sigma_3 Z}\right]. \tag{63}$$

And (63) is written as

$$\lambda_3 = A_1 e^{-\delta t}, \tag{64}$$

where

$$A_1 = -\left[\frac{\left(\alpha - \left(\beta/qL^2\right)\right)(\delta + \sigma_{30} L s) - \alpha q E}{\sigma_3 Z}\right]. \tag{65}$$

From (67) and the third equation of (58),

$$-\delta A_1 e^{-\delta t} = -\lambda_2(-\sigma_2 P) - \lambda_3(\gamma_2 P - \mu_2 - 2\sigma_3 L) - \lambda_4(\gamma_3 L). \tag{66}$$

Substituting (20) into (66), we obtain

$$\lambda_2 = -e^{-\delta t}\left[\frac{\delta A_1 - \left(\alpha - \left(\beta/qL^2\right)\right)}{\sigma_2 P}\right]. \tag{67}$$

And (67) is written as

$$\lambda_2 = A_2 e^{-\delta t}, \tag{68}$$

where

$$A_2 = -\left[\frac{\delta A_1 - \left(\alpha - \left(\beta/qL^2\right)\right)}{\sigma_2 P}\right]. \tag{69}$$

From equation (71) and the second equation of (58),

$$-\delta A_2 e^{-\delta t} = \lambda_1\sigma_1 N - \lambda_3\gamma_2 Z. \tag{70}$$

Substituting (20) into (66), we obtain

$$\lambda_1 = -e^{-\delta t}\left[\frac{\delta A_2 - A_1\gamma_2 Z}{\sigma_1 N}\right]. \tag{71}$$

And (67) is written as

$$\lambda_1 = A_3 e^{-\delta t}, \tag{72}$$

where

$$A_3 = -\left[\frac{\delta A_2 - A_1\gamma_2 Z}{\sigma_1 N}\right]. \tag{73}$$

From (72), the first equation of (18), and (58),

$$-\delta A_3 e^{-\delta t} = -\lambda_1\left(\frac{-a}{N}\right) - \lambda_2\gamma_1 P. \tag{74}$$

$$A_3 = \frac{\gamma_1 P A_2}{a/N + \delta}. \tag{75}$$

Substituting the values of A_2, A_1 into (75), we obtain

$$E = \frac{\left(\alpha q L^2 - \beta\right)\left((a+\delta N)\left(\gamma_2 P\sigma_2 Z(\delta+\sigma_{30}L) + \delta\left(\delta^2 + \sigma_3 Z + \delta\sigma_{30}L\right)\right) + \gamma_1 P\sigma_1 N^2\left(\sigma_3 Z + \delta(\delta+\sigma_{30}L)\right)\right)}{\alpha q^2 L^2\left((a+\delta N)\left(\delta^2 + \gamma_2 P\sigma_2 Z\right) + \gamma_1\delta P\sigma_1 N^2\right)}. \tag{76}$$

The optimal solution $(N_\delta, P_\delta, Z_\delta, L_\delta)$ and the optimal harvesting effort $E = E_\delta$ are obtained by solving (18)–(21) with (76). Solving (18)–(21) and (76) using the same default parameter values and with $\alpha = 0.86$, $\beta = 0.001$, and $\delta = 0.12$, we obtain the optimal equilibrium $(N_\delta, P_\delta, Z_\delta, L_\delta) = (0.13448, 503.543, 0.0695343, 128.543)$ and the optimal effort, $E^* = 15393.9$ boat nights. The optimal number of boats is $(15393.9/30.5) \approx 505$, in the Lake Kariba fishery. Since the Zimbabwean and Zambian sides of the Lake are in the ratio 0.55: 0.45, we therefore recommend 278 boats and 227 on the Zimbabwean and Zambian sides of the kapenta fishery, respectively. The optimal number of fishing units of 505 is in agreement with the recommended 500 in the Lake Kariba fishery [12]. The plot of kapenta for different values of E is shown in Figure 7.

The rate of change of E with α in (77) is positive implying that if the price per unit of harvested kapenta increases the effort increases, for fixed β. This means that as the price rises of kapenta, the number of fishing vessels is likely to increase in the fishery.

$$\frac{\partial E}{\partial \alpha} = \frac{\beta\left((a+\delta x)\left(\gamma_2 p\sigma_2 w(\delta+\sigma_{30}y) + \delta\left(\delta^2 + \sigma_3 w + \delta\sigma_{30}y\right)\right) + \gamma_1 p\sigma_1 x^2\left(\sigma_3 w + \delta(\delta+\sigma_{30}y)\right)\right)}{\alpha^2 q^2 y^2\left((a+\delta x)\left(\delta^2 + \gamma_2 p\sigma_2 w\right) + \gamma_1\delta p\sigma_1 x^2\right)}. \tag{77}$$

The rate of change of E with β in (78) is negative implying that if the utilised cost per unit effort increases the effort decreases, for fixed α. If the cost of fishing rises, then the number of fishing vessels in the fishery can decline.

$$\frac{\partial E}{\partial \beta} = -\frac{(a+\delta x)\left(\gamma_2 p\sigma_2 w(\delta+\sigma_{30}y) + \delta\left(\delta^2 + \sigma_3 w + \delta\sigma_{30}y\right)\right) + \gamma_1 p\sigma_1 x^2\left(\sigma_3 w + \delta(\delta+\sigma_{30}y)\right)}{\alpha q^2 y^2\left((a+\delta x)\left(\delta^2 + \gamma_2 p\sigma_2 w\right) + \gamma_1\delta p\sigma_1 x^2\right)}. \tag{78}$$

3. Results

3.1. Data Fitting. The Fourier series equations (79)–(82) were used in the data fitting.

$$f(t) = \frac{a_0}{2} + \sum_{n=1}^{\infty} a_n \cos(nt) + \sum_{n=1}^{\infty} b_n \sin(nt), \tag{79}$$

where

$$a_0 = \frac{1}{\pi}\int_{-\pi}^{\pi} f(t)\mathrm{d}t, \tag{80}$$

$$a_n = \frac{1}{\pi}\int_{-\pi}^{\pi} f(t)\cos(nt)\mathrm{d}t, \tag{81}$$

$$b_n = \frac{1}{\pi}\int_{-\pi}^{\pi} f(t)\sin(nt)\mathrm{d}t. \tag{82}$$

and $n = 1, 2, 3, 4, \ldots$ [33].

A Fourier series with an order of fit of $n = 2$ in (83) was used in MATLAB R2016a to estimate the parameters of the total nitrogen data for the period from April 2014 to December 2017. The monthly averages from January to December were used in the data fitting.

$$\begin{aligned} f(t) = {} & a_0 + a_1\cos(\omega t) + b_1\sin(\omega t) \\ & + a_2\cos(2\omega t) + b_2\sin(2\omega t). \end{aligned} \tag{83}$$

The parameter estimates of (83) are shown in Table 1.

The actual and fitted plots of monthly average total nitrogen are shown in Figure 8.

The fitted models in (83) goodness of fit statistics are sum of squared estimate of errors (SSE) $= 7.615 \times 10^4$, $R^2 = 0.6095$, and root mean square error (RMSE) = 112.7.

Factoring trigonometric functions in (83) using Wolfram Mathematica 11.0 results in

$$f(t) = 11.03\,(56.1015 + 10.9614\,\sin(0.0913563 + 0.6106t) - 5.21772\,\sin(0.878172 - 1.2212t)). \tag{84}$$

and we obtain

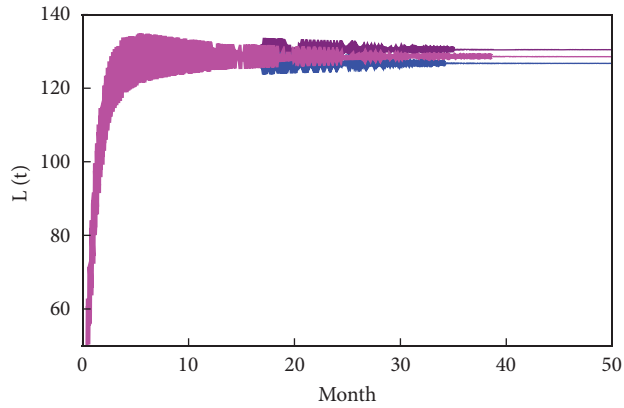

Figure 7: Time series of Limnothrissa miodon for varying fishing effort for model system (2) with $E = 7625$ (colour purple), $E = 15250$ (colour magenta), and $E^* = 15394$ (colour blue).

Table 1: Fourier coefficients from data fitting.

Coefficient	Estimate	95% confidence bounds
a_0	618.8	(533.1, 704.6)
a_1	11.03	(−166.4, 188.5)
b_1	120.4	(4.689, 236.1)
a_2	−44.29	(−195.6, 107.1)
b_2	36.75	(−93.15, 166.6)
ω	0.6106	(0.4416, 0.7795)

$$f(t) = 618.8(1 + 0.195385\ \sin(0.6106t + 0.0913563) + 0.0930049\ \sin(1.2212t + 0.878172)). \quad (85)$$

Then (85) can be generalised as

$$f(t) = a(1 + b\ \sin(\omega t + \varphi_1) + c\ \sin(2\omega t + \varphi_2)). \quad (86)$$

3.2. Numerical Simulations. Model parameters of system (2) and their interpretations are shown in Table 2. Besides the catchability coefficient q of L, the description, symbol, value, and source of the parameters and coefficients in Table 2 are the same as those used in the study by Mutasa et al. [28], except that the parameters are monthly parameters. Numerical simulations for system (2) are done in Wolfram Mathematica 11.0 using a fourth-order Runge–Kutta numerical scheme. The units of the variables N, P, Z, and L are μgl^{-1}.

3.2.1. Nonautonomous Model. For the set of the default parameters, the phase portraits showing the time series of nutrients, phytoplankton, zooplankton, and kapenta with harvesting are shown in Figures 9(a)–9(d), respectively. Figure 9 shows stable periodic solutions of period 1 corresponding to the default parameter values. For varying initial conditions, all initial conditions lead to periodic solutions. Different initial conditions lead to the same periodic solution curve and therefore we have a stable limit cycle in the phase space. The time series for zooplankton initially has irregular fluctuations showing that the density of zooplankton is highly variable and eventually stabilizes into a periodic orbit after 40 months. This could be attributed to the initial phase in the lake when the fishery started to operate and then eventually stabilized after some time.

Figures 10(a)–10(b) show oscillatory dynamics in the phase portraits of the nutrient and phytoplankton; phytoplankton and zooplankton; zooplankton and Limnothrissa miodon; phytoplankton, zooplankton, and Limnothrissa miodon dynamics for system (2), respectively. The phase portraits show that the equilibrium point at $\mathscr{E}_* = (0.134, 503.68, 0.0694, 128.578)$ (point with colour yellow) for the autonomous model is enclosed by the periodic solutions of the nonautonomous model, but the system does not go to the equilibrium point.

3.2.2. Effects of Nutrients and Fishing Effort for the Nonautonomous Model. For the set of the default parameters, Figures 11(a) and 11(b) illustrate the effect of varying the inflow of nutrients parameter a in model (2) on the dynamics of Limnothrissa miodon with $E = 15250$. Figures 11(c) and 11(d) illustrate the effect of varying fishing effort in model (2) on the dynamics of Limnothrissa miodon.

Simulation results from Figures 11(a)–11(d) show that the abundance of Limnothrissa miodon is more closely related to the availability of nutrients than to harvesting. Marshall [42] and Paulsen [43] in their studies showed that the abundance of Limnothrissa miodon is mainly due to river inflow and the availability of food compared to harvesting.

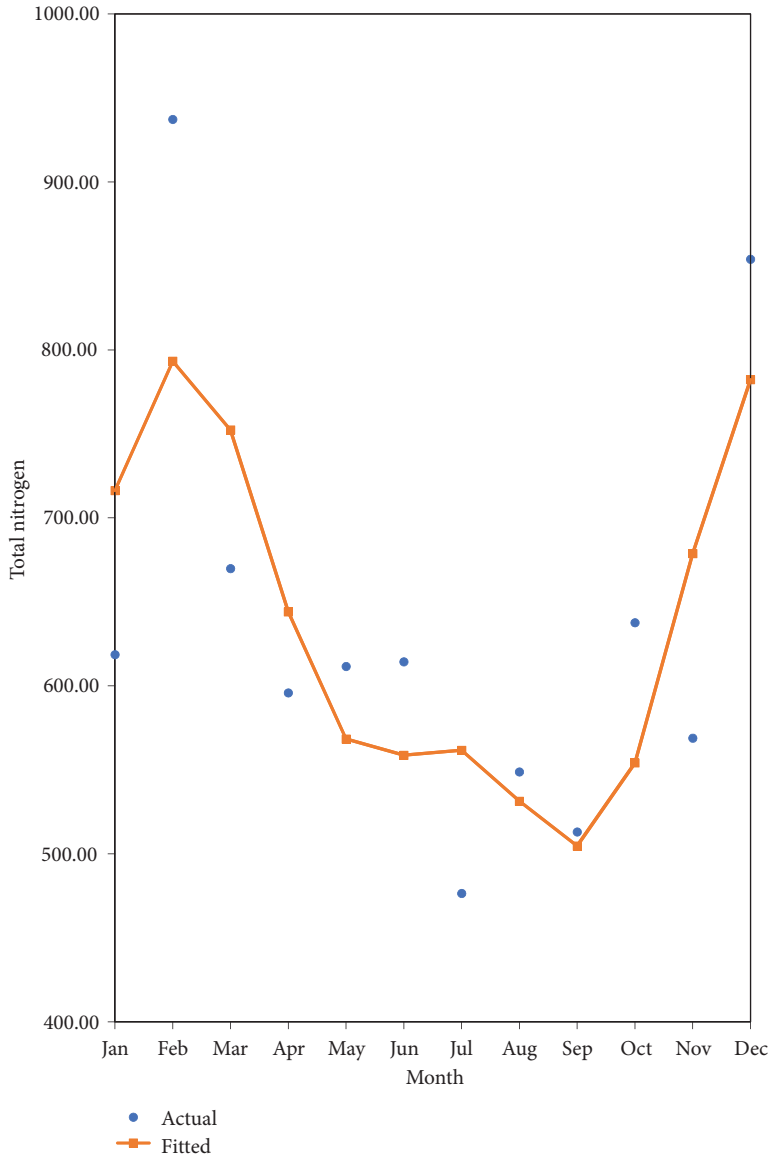

Figure 8: Monthly average of total nitrogen (μg / l) and fitted curve.

Table 2: Model parameters and their interpretations.

Symbol	Definition	Value	Source
μ_0	N natural depletion rate coefficient	$0.2924\,\text{month}^{-1}$	
σ_1	P uptake rate of N	$9.13751\,\text{l}\,\mu\text{g}^{-1}\text{month}^{-1}$	[34]
ϕ_1	P conversion coefficient of N	1	
μ_1	P natural depletion rate coefficient	$3.965, 0.976 - 2.44, 13.4505\,\text{month}^{-1}$	[13, 35, 36]
σ_2	Z grazing rate of P	$18.3 - 42.7, 17.08, 3.05 - 21.045\,\text{l}\,\mu\text{g}^{-1}\text{month}^{-1}$	[13,37, 38]
ϕ_2	Z conversion coefficient of P grazing	$0.2 - 0.75, 1.5$	[39, 40]
μ_2	Z natural depletion rate coefficient	$0.305, 1.6104\,\text{month}^{-1}$	[13, 41]
σ_3	L grazing rate of Z	$14.335\,\text{l}\,\mu\text{g}^{-1}\text{month}^{-1}$	
σ_{30}	L crowding effect coefficient	$0.000152\text{l}\,\mu\text{g}^{-1}\text{month}^{-1}$	[13]
ϕ_3	L conversion coefficient of Z grazing	1	
μ_3	L natural mortality	$0.2928, 0.2745, 0.7625 - 1.11935\,\text{month}^{-1}$	[7, 9, 13]
q	L catchability coefficient	0.00000153	[17]

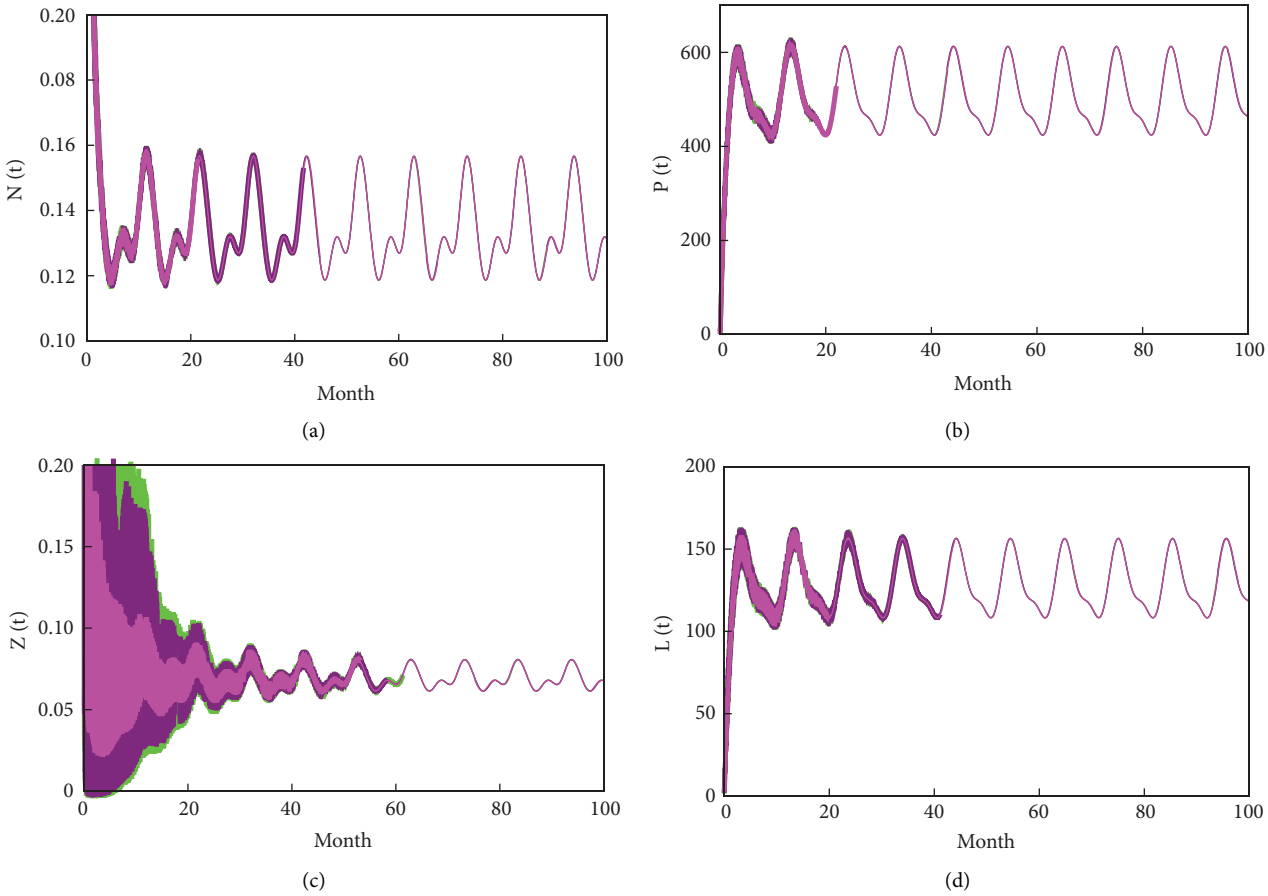

Figure 9: Phase portrait showing the time series of (a) nutrients; (b) phytoplankton; (c) zooplankton; (d) Limnothrissa miodon for model (2) and assumed initial condition: $N(0) = 9.5, P(0) = 6.5, Z(0) = 3.5, L(0) = 1.5$ (time series with colour green); $N(0) = 10, P(0) = 7, Z(0) = 4, L(0) = 2$ (time series with colour purple); $N(0) = 10.5, P(0) = 7.5, Z(0) = 4.5, L(0) = 2.5$ (time series with colour magenta); using the default parameter.

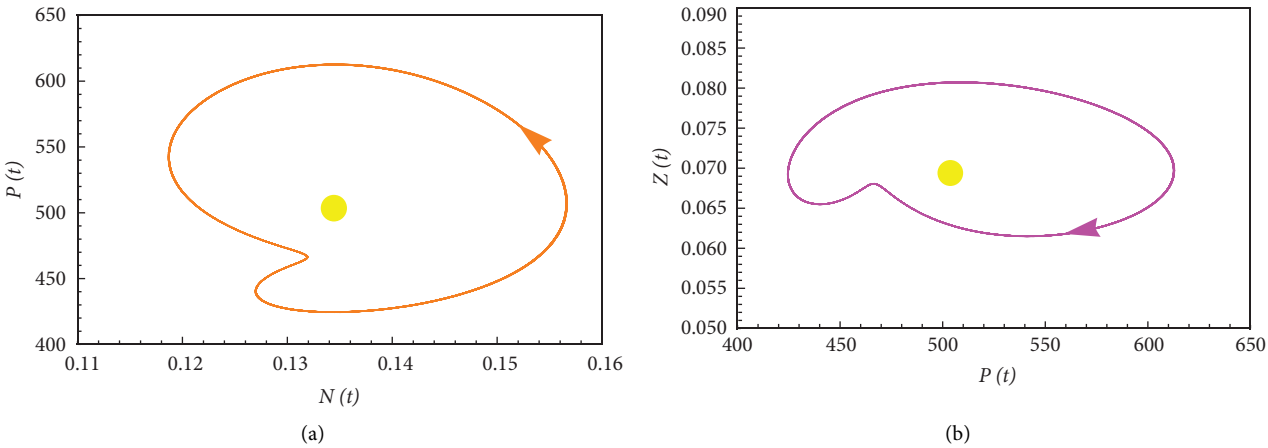

Figure 10: Continued.

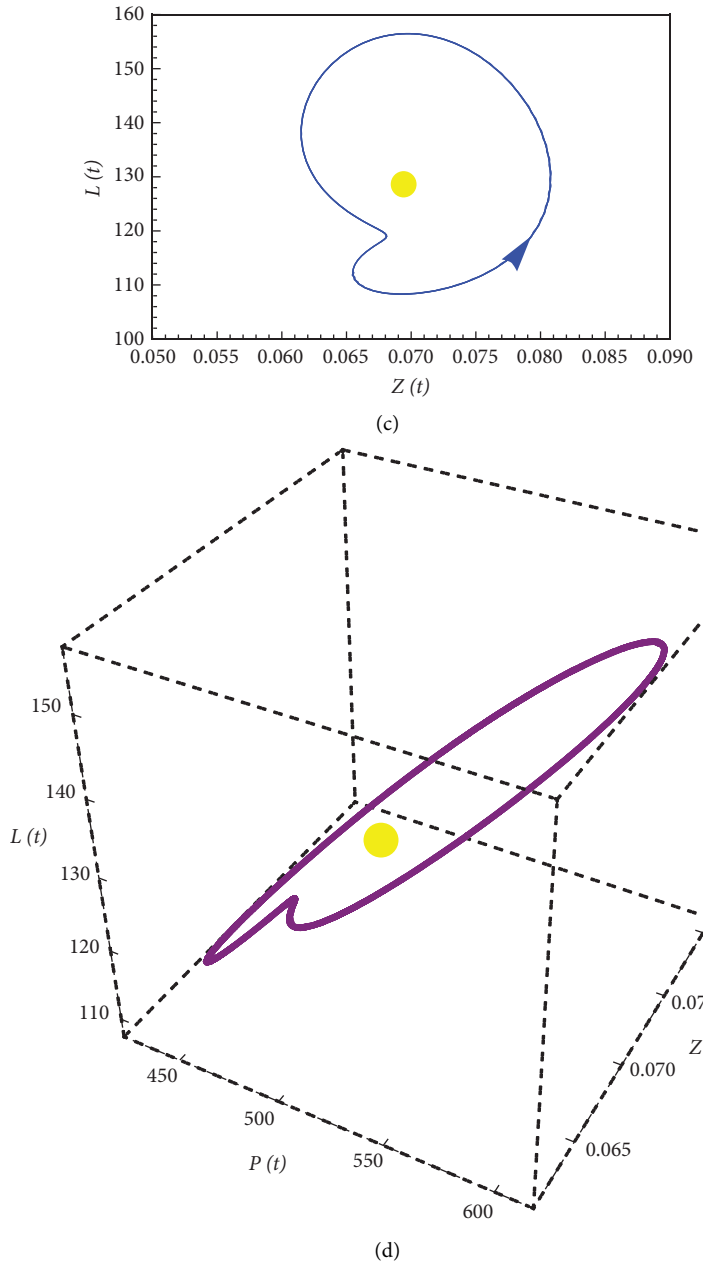

FIGURE 10: Phase portrait showing the dynamics of (a) phytoplankton and nutrients; (b) zooplankton and phytoplankton; (c) Limnothrissa miodon and zooplankton; (d) Limnothrissa miodon, zooplankton, and phytoplankton for model system (2) with assumed initial condition: $N(0) = 10, P(0) = 7, Z(0) = 4, L(0) = 2$ using the default parameter values.

4. Discussion

We developed and examined the dynamics of a mathematical model that includes nutrients, phytoplankton, zooplankton, and Limnothrissa miodon in this paper. The phytoplankton growth rate, phytoplankton mortality, phytoplankton grazing, zooplankton growth rate, zooplankton mortality, grazing on zooplankton, and Limnothrissa miodon mortality are assumed to be Holling type-I forms. Theoretical analysis, including the positivity and existence of model solutions (2), is investigated. We obtained the autonomous model's critical points and examined their stabilities. The equilibrium points' local and global stability conditions are established. The autonomous and nonautonomous models were numerically simulated. The study's highlights are as follows:

(i) The application of a dynamical system to the food chain, nutrients $\longrightarrow$ phytoplankton $\longrightarrow$ zooplankton $\longrightarrow$ Limnothrissa miodon, is used to demonstrate the qualitative behavior of Limnothrissa miodon in the presence of harvesting. Given a set of parameter values and initial conditions, the phase portraits are damped oscillations

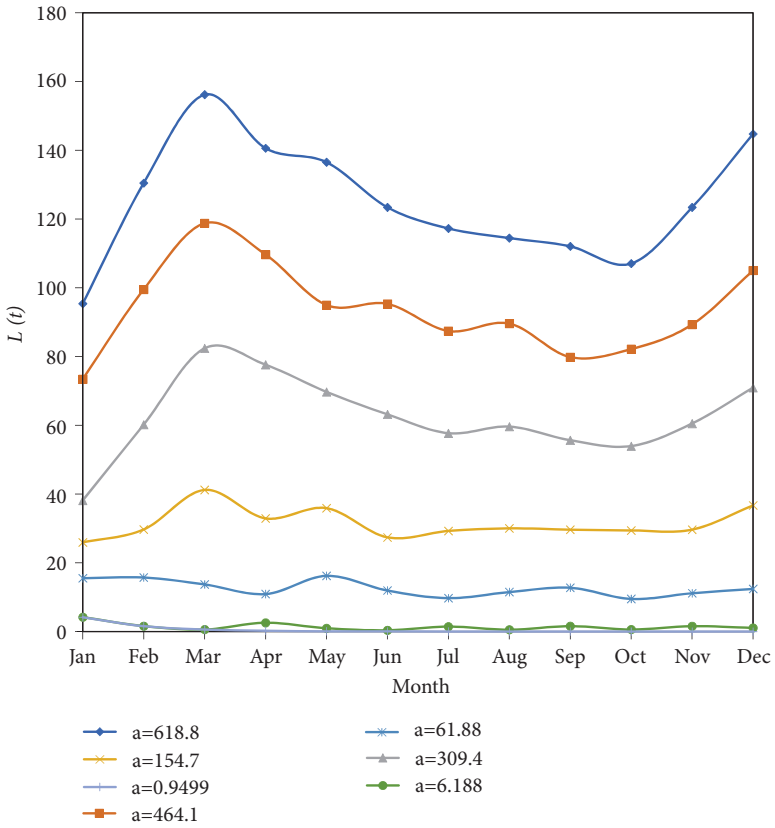

(a)

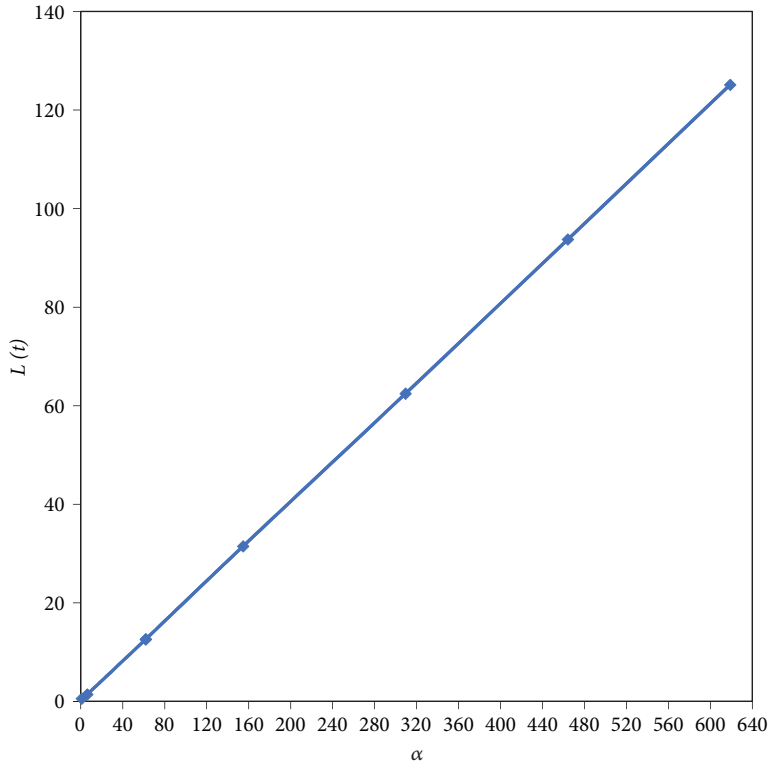

(b)

Figure 11: Continued.

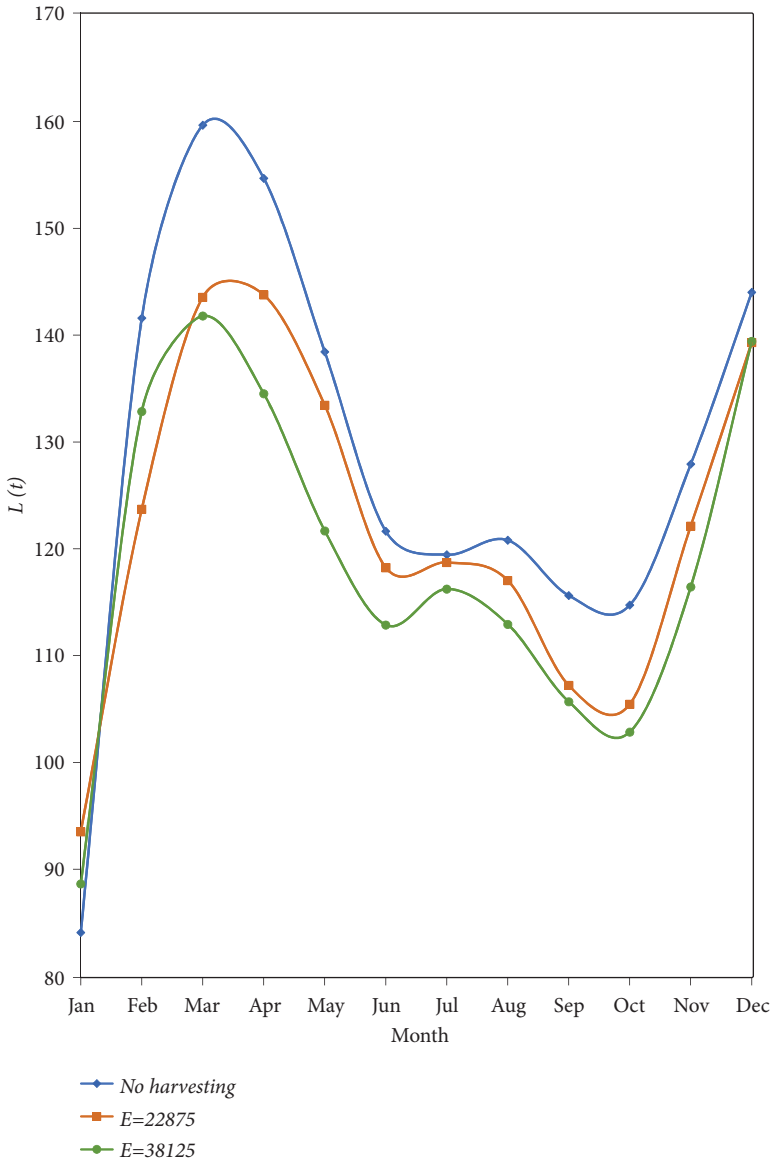

(c)

Figure 11: Continued.

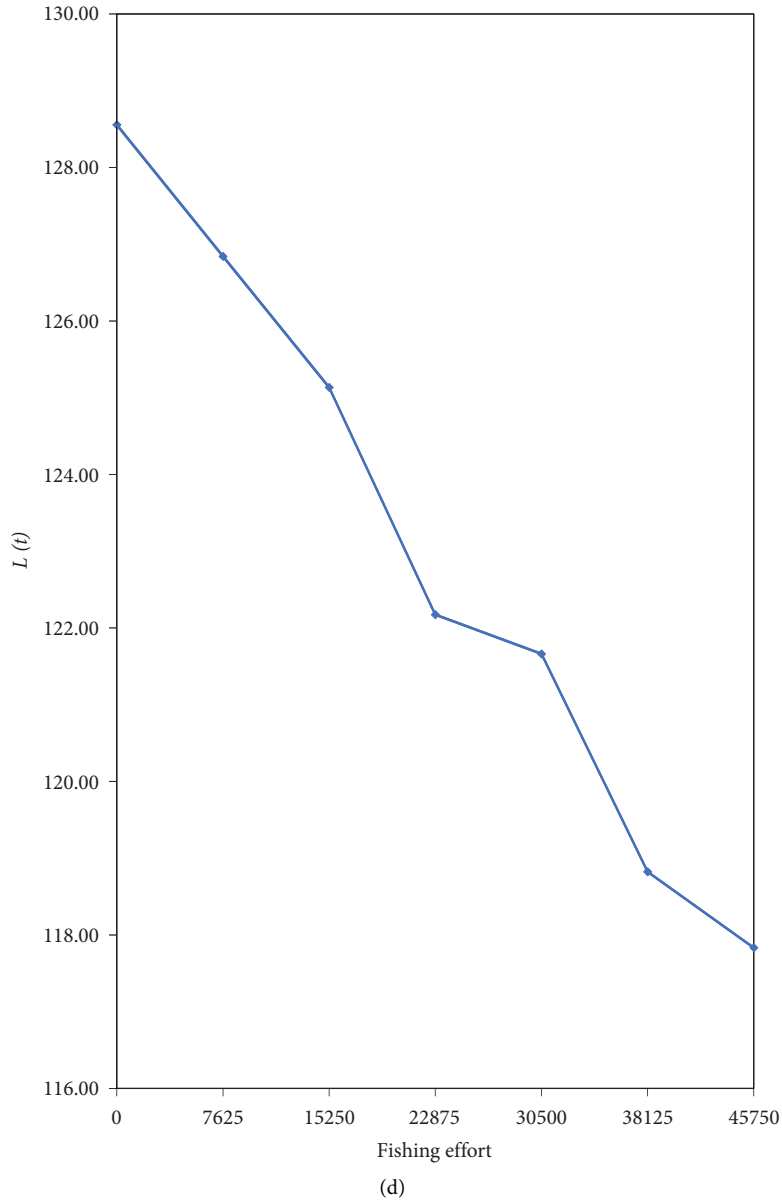

FIGURE 11: (a) Time series of Limnothrissa miodon for varying a for model system (2); (b) 12-month average plot of Limnothrissa miodon for varying a; (c) time series of Limnothrissa miodon for varying fishing effort for model system (2) with $E = 0$, $E = 22875$, and $E = 38125$; (d) 12-month average plot of Limnothrissa miodon to fishing effort and with assumed initial condition: $N(0) = 10, P(0) = 7, Z(0) = 4, L(0) = 2$ using the default parameter values.

for the autonomous model and show periodic behavior for the nonautonomous model.

(ii) For the autonomous model's local stability analysis, the theoretical results agree with the numerical simulations in that the coexistence equilibrium is stable if certain conditions are satisfied. If the equilibrium $\mathscr{E}_*$ is feasible, it is globally unstable. Numerical results show that the nonautonomous model in Lake Kariba has a stable limit cycle.

(iii) Data fitting results for the period 2015 to 2017 show that there are two notable peaks in April and August in Lake Kariba which correspond to the inflow of nutrients from river inflow and runoff and nutrient reloading, respectively.

(iv) The rate of nutrient inflow has a positive effect on the Limnothrissa miodon abundance. Numerical simulations of system (2) show that Limnothrissa miodon abundance is negatively affected by harvesting.

(v) Abundance of Limnothrissa miodon has been shown to vary seasonally in relation to food abundance in Lake Kariba.

(vi) Optimal control results from the autonomous model show 505 optimal fishing units, showing that currently there is overcapacity in Lake Kariba.

(vii) A maximum sustainable annual catch of 34669 tonnes per year in Lake Kariba is obtained for the autonomous model.

(viii) The Limnothrissa miodon will flourish in the lake for model system (2) as long as the harvesting rate is less than 34669 tonnes per year, with parameter values as shown in Table 2. As a result, the harvesting rate is critical to Lake Kariba's productivity.

(ix) Simulation results show that kapenta abundance is more closely related to inflow of nutrients than to harvesting.

5. Conclusions

The basic kapenta model [28] is extended to include harvesting by fishing vessels. The kapenta fishery in Lake Kariba provides a significant source of income for many people in Zimbabwe and Zambia. As a result, fishery management is critical to the fishery's long-term survival, as it is a major source of income for fishing cooperatives, wholesalers, retailers, and the Lake Kariba community. Many people use kapenta as a relish and a source of protein. Lake Kariba kapenta fishing is in jeopardy due to dwindling fish populations. Kapenta harvesting must be done in a sustainable manner so that the resource does not become extinct. As a result, mathematical modelling of the kapenta model with harvesting provided us with insight into the dynamics of the Lake Kariba kapenta fishery. We developed a mathematical model for kapenta harvesting with the goal of ensuring that sustainable levels of kapenta are maintained. Dynamical systems have not been used to investigate how kapenta fish populations in a lake are described and influenced by harvesting. We were able to qualitatively explain the impact of harvesting by developing a mathematical model and analyzing it. Once we fully comprehend the dynamics, we will be able to intervene in order to maintain sustainable levels of kapenta fish. Currently there is overcapacity in Lake Kariba, and the kapenta is being overexploited. Based on our optimal control results, we recommend 505 fishing vessels, 278 for the Zimbabwean side and 227 for the Zambian side of Lake Kariba.

Data Availability

The data used to support the study's findings are included in the article.

Conflicts of Interest

The authors of this study have no conflicts of interest.

Acknowledgments

The authors would like to express their gratitude to the Lake Kariba Fisheries Research Institute and the University of Zimbabwe Lake Kariba Research Station for providing the data used in this study. Dr. Nobuhle Ndlovu, Ms. Adroid T. Chakandinakira, and Ms. P Chirozva deserve special recognition. This study was supported by the National University of Science and Technology, Research Board Grant number RDB/90/18.

References

[1] G. Bell-Cross and B. Bell-Cross, "Introduction of limnothrissa miodon and limnocaridina tanganicae from lake tanganyika into Lake Kariba," *Fish Res Bull Zambia*, vol. 5, pp. 207–214, 1971.

[2] M. Chali, C. G. Musuka, and B. Nyimbili, "The impact of fishing pressure on kapenta (limnothrissa miodon) production in Lake Kariba, Zambia: a case study of Siavonga District," *International Journal of Agriculture, Forestry and Fisheries*, vol. 2, no. 6, pp. 107–116, 2014.

[3] G. Paulet, "Kapenta Rig Survey of the Zambian waters of Lake Kariba. SF/2014/45 programme for the implementation of a regional fisheries strategy for the eastern and southern Africa Indian ocean region," 2013, https://www.coi-ioc.org/.

[4] S. M. McLachlan, "The influence of lake level fluctuations and the thermocline on water chemistry in two gradually shelving areas of Lake Kariba, Central Africa," *Archiv für Hydrobiologie*, vol. 66, no. 4, pp. 499–510, 1970.

[5] B. E. Marshall, "The influence of river flow on pelagic sardine catches in Lake Kariba," *Journal of Fish Biology*, vol. 20, no. 4, pp. 465–469, 1982.

[6] B. E. Marshall, "Growth and mortality of the introduced Lake Tanganyika clupeid, Limnothrissa miodon, in Lake Kariba," *Journal of Fish Biology*, vol. 31, no. 5, pp. 603–615, 1987.

[7] J. Moreau, J. Munyandorero, and B. Nyakageni, "Evaluation des paramètres démographiques chez Stolothrissa tanganykae et Limnothrissa miodon du lac Tanganyka," *SIL Proceedings, 1922-2010*, vol. 24, no. 4, pp. 2552–2558, 1991.

[8] L. Kinadjian, C. Mwula, K. Nyikahadzoi, and N. Songore, "Bioeconomic modelling of kapenta fisheries on Lake Kariba," Report/Rapport: SFFAO/2014/22, FAO-SmartFish Programme of the Indian Ocean Commission, Ebene, Mauritius, 2014.

[9] "Anonymous. Working group on the assessment of kapenta (Limnothrissa miodon) in Lake Kariba (Zambia and Zimbabwe) ," vol. 43, Lake Kariba Fisheries Research Institute, Kariba, Zimbabwe, 1992, Zambia/Zimbabwe SADC Fisheries Project Report N411996.

[10] K. L. Cochrane, "Seasonal fluctuations in the catches of Limnothrissa miodon (boulenger, 1906) in Lake Kariba," *Lake Kariba Fisheries Research Institute Project Report*, vol. 29, p. 163, 1978.

[11] B. E. Marshall, "Seasonal and annual variations in the abundance of pelagic sardines in Lake Kariba, with special reference to the effects of drought," *Archiv fur Hydrobiologie, Stuttgart*, vol. 112, no. 3, pp. 399–409, 1988.

[12] F. AO. Fifth, "Technical consultation on development and management of the fisheries of Lake Kariba," Report, No. Rome, FAO. 2012. 35p, pp. 11–13, FAO-fisheries and aquaculture 4p, Siavonga, Zambia, 2012.

[13] C. Machena, J. Kolding, and R. A. Sanyanga, "A preliminary assessment of the trophic structure of Lake Kariba, Africa," *Trophic Models of Aquatic Ecosystems. International center for living aquatic resources management conference proceedings*, vol. 26, p. 1307, 1993.

[14] C. H. D. Magadza, "Indications of the effects of climate change on the pelagic fishery of Lake Kariba, Zambia-Zimbabwe," *Lakes & Reservoirs: Science, Policy and Management for Sustainable Use*, vol. 16, no. 1, pp. 15–22, 2011.

[15] L. Madamombe, "The economic development of the kapenta fishery Lake Kariba (Zimbabwe/Zambia)," Masters Thesis, Norwegian College of Fishery Science. University of Troms, Troms, Norway, 2002.

[16] H. G. Mudenda, "Sustainability and management of the Lake Kariba kapenta fishery," Institute for Policy Studies (IPS). The Zambia national farmers union (ZNFU), Zambia, 2010.

[17] I. H. Tendaupenyu and H. D. Pyo, "A comparative analysis of maximum entropy and analytical models for assessing kapenta (Limnothrissa miodon) stock in Lake Kariba," *Environmental and Resource Economics Review*, vol. 26, no. 4, pp. 613–639, 2017.

[18] C. W. Clark and M. Mangel, "Of schooling and the purse seine tuna fisheries," *Fishery Bulletin*, vol. 77, no. 2, p. 317, 1979.

[19] M. B. Schaefer, "A study of the dynamics of the fishery for yellowfin tuna in the eastern tropical Pacific Ocean," *Inter-American Tropical Tuna Commission Bulletin*, vol. 2, no. 6, pp. 243–285, 1957.

[20] L. V. Idels and M. Wang, "Harvesting fisheries management strategies with modified effort function," *International Journal of Modelling, Identification and Control*, vol. 3, no. 1, p. 8387, 2008, https://doi.org/10.1504/IJMIC.2008.018188.

[21] M. R. Ndebele-Murisa, *An analysis of primary and secondary production in Lake Kariba in a changing climate*, Ph.D. thesis, University of the Western Cape, Bellville, South Africa, 2011.

[22] L. Kinadjian, C. Mwula, K. Nyikahadzoi, and N. Songore, *Report on the Bioeconomic Modelling of Kapenta Fisheries on Lake Kariba. SmartFish Programme of the Indian Ocean Commission, FAO Fisheries Management*, component, pp. 1–108, Ebene, Mauritius, 2014.

[23] B. E. Marshall, "A preliminary assessment of the biomass of the pelagic sardine Limnothrissa miodon in Lake Kariba," *Journal of Fish Biology*, vol. 32, no. 4, pp. 515–524, 1988, https://doi.org/10.1111/j.1095-8649.1988.tb05391.x.

[24] T. Lindem, "Results from the hydroacoustic survey Lake Kariba," Zimbabwe/Zimbabwe SADC Fisheries Project, Department of Physics, University of Oslo, Norway, 1988.

[25] T. Lindem, "Results from the hydroacoustic survey Lake Kariba," Zimbabwe/Zimbabwe SADC Fisheries Project, Department of Physics, University of Oslo, Norway, 1992.

[26] J. M. Mafuca, "Preliminary results of the hydroacoustic survey conducted on Lake Kariba," Report/Rapport: SFFAO/2014/33, 2014.

[27] N. Songore, A. Moyo, and M. Mugwagwa, *Annual Statistical Report, Report No. 100*, Lake Kariba Fisheries Research Institute, Kariba, Zimbabwe, 2000.

[28] F. K. Mutasa, B. Jones, and S. D. Hove-Musekwa, "Modelling and analysis of Limnothrissa miodon population in a Lake," *Chaos, Solitons & Fractals: The Interdisciplinary Journal of Nonlinear Science, and Nonequilibrium and Complex Phenomena*, vol. 136, 2020, https://doi.org/10.1016/j.chaos.2020.109844.

[29] C. S. Holling, "The components of predation as revealed by a study of small-mammal predation of the European pine sawfly," *The Canadian Entomologist*, vol. 91, no. 5, pp. 293–320, 1959.

[30] L. Perko, *Differential Equations and Dynamical Systems*, vol. 7, Springer Science & Business Media, Berlin, Germany, 2013..

[31] A. Korobeinikov, "Lyapunov functions and global stability for SIR and SIRS epidemiological models with non-linear transmission," *Bulletin of Mathematical Biology*, vol. 68, no. 3, pp. 615–626, 2006.

[32] R. K. Upadhyay, S. K. Tiwari, and P. Roy, "Complex dynamics of wetland ecosystem with nonlinear harvesting: application to Chilika Lake in Odisha, India," *International Journal of Bifurcation and Chaos*, vol. 25, no. 07, p. 1540016, 2015.

[33] E. W. Weisstein, "Fourier Series." from MathWorld–A Wolfram Web Resource," https://mathworld.wolfram.com/FourierSeries.html.

[34] G. T. Orlob, "Mathematical modeling of water quality: streams, Lakes and reservoirs," *John Wiley & Sons*, vol. 12, 1983.

[35] L. Ding, Y. Pang, and L. Li, "Simulation study on algal dynamics under different hydrodynamic conditions," *Acta Ecologica Sinica*, vol. 25, pp. 1863–1868, 2005.

[36] A. Edwards and J. Brindley, "Zooplankton mortality and the dynamical behaviour of plankton population models," *Bulletin of Mathematical Biology*, vol. 61, no. 2, pp. 303–339, 1999, https://doi.org/10.1080/02681119608806231.

[37] S. Kartal, M. Kar, N. Kartal, and F. Gurcan, "Modelling and analysis of a phytoplankton-zooplankton system with continuous and discrete time," *Mathematical and Computer Modelling of Dynamical Systems*, vol. 22, no. 6, pp. 539–554, 2016.

[38] L. V. Stelmakh, I. I. Babich, S. Tugrul, S. Moncheva, and K. Stefanova, "Phytoplankton growth rate and zooplankton grazing in the western part of the Black Sea in the autumn period," *Oceanology*, vol. 49, no. 1, pp. 83–92, 2009.

[39] J. Brindley, "Oscillatory behaviour in a three-component plankton population model," *Dynamics and Stability of Systems*, vol. 11, no. 4, pp. 347–370, 1996.

[40] S. Pal and A. Chatterjee, "Dynamics of the interaction of plankton and planktivorous fish with delay," *Cogent Mathematics*, vol. 2, no. 1, Article ID 1074337, 2015.

[41] K. Kulinski, A. Maciejewska, L. Dzierzbicka-Glowacka, and J. Pempkowiak, "Parameterisation of a zero-dimensional pelagic detritus model, gdansk deep, baltic sea," *Rocz Ochr Sr*, vol. 13, pp. 187–206, 2011.

[42] B. E. Marshall, "Small pelagic fishes and fisheries in African inland waters," *Committee for Inland Fisheries of Africa Technical Paper*, vol. 14, p. 25, 1984.

[43] H. Paulsen, "The feeding habits of kapenta, Limnothrissa miodon in Lake Kariba," Technical Report, Zambia/Zimbabwe SADC Fisheries Project Report 30, Zimbabwe, 1994.